



Cite this: *New J. Chem.*, 2021, 45, 5659

Chemoselective hydrogenation of cinnamaldehyde over a tailored oxygen-vacancy-rich Pd@ZrO₂ catalyst†

Komal N. Patil,^a Divya Prasad,^a Jayesh T. Bhanushali,^a Bhalchandra Kakade,^b Arvind H. Jadhav[✉]*^a and Bhari Mallanna Nagaraja[✉]*^a

Selective hydrogenation of cinnamaldehyde to hydrocinnamaldehyde is captivating due to its industrial relevance. Herein, a two-step synthesis method was adopted to develop oxygen vacancies in Pd@ZrO₂ catalysts. The oxygen vacancies were developed in Pd@ZrO₂ catalysts during impregnation of Pd which was confirmed by XPS and HR-TEM analyses. The characterization results revealed that there was a synergistic role of oxygen vacancies and nano-sized active Pd metals in Pd@ZrO₂ catalysts that assisted in achieving selectivity for hydrocinnamaldehyde which has been discussed in this study. We also studied the effects of different reaction parameters which revealed that 4 wt% Pd loading in a Pd@ZrO₂ catalyst provided enough active sites for complete conversion of CAL. Additionally, 100 °C temperature and 10 bar H₂ pressure provided enough energy for effective collisions and activation of reactants and catalysts to form the desired product in a reaction time of 9 h. Therefore, a defect-rich 4-Pd@ZrO₂ catalyst demonstrated complete CAL conversion with 86% yield towards HCAL which is the best result amongst various Pd@ZrO₂ catalysts with different Pd loading investigated for the hydrogenation of cinnamaldehyde. Moreover, a plausible mechanism was proposed to support the chemoselective hydrogenation of cinnamaldehyde over a 4-Pd@ZrO₂ catalyst. Along with high catalytic performance, the 4-Pd@ZrO₂ catalyst also showed impressive recyclability performance for up to six recycles. Thus, the oxygen-vacancy-rich Pd@ZrO₂ can be considered as an efficient catalyst for the chemoselective hydrogenation of cinnamaldehyde.

Received 16th November 2020,
Accepted 21st February 2021

DOI: 10.1039/d0nj05595f

rsc.li/njc

1. Introduction

Catalytic hydrogenation reactions have attracted research interest due to their process versatility and green credentials compared to a typical chemical reduction process that involves stoichiometric

quantities of a reducing agent.¹ Under this perspective, catalysis has turned out to be the foundation stone of chemical industries when carrying out hydrogenation reactions using molecular hydrogen.² The constant development in the field of catalysis in compliance with green chemistry principles to perform these reactions under moderate reaction conditions permitting high activity and selectivity is of high priority these days.³ Among all the aspects of catalysis, chemoselectivity is highly targeted to achieve atom efficiency by focusing on single product formation and thus minimizing waste generation.⁴ In this perspective, chemoselective hydrogenation of α,β -unsaturated aldehydes, classically cinnamaldehyde, using H₂ can be considered as a clean process with close to 100% atom efficiency.⁵ Selective hydrogenation of cinnamaldehyde is of utmost importance amongst several industrial hydrogenation processes and has attracted extraordinary research interest because it provides both scientific and industrial significance.^{2,6}

Typically, hydrogenation of cinnamaldehyde may lead to the formation of cinnamyl alcohol (COL) (selective hydrogenation of C=O), hydrocinnamaldehyde (HCAL) (selective hydrogenation of C=C) and/or hydrocinnamyl alcohol (HCOL) (hydrogenation

^a Centre for Nano and Material Science (CNMS), JAIN (Deemed-to-be University), Jain Global Campus, Bangalore-562112, India.

E-mail: j.arvind@jainuniversity.ac.in, jadhav.ah@gmail.com, bm.nagaraja@jainuniversity.ac.in, nagarajabhari@gmail.com

^b Department of Chemistry, SRM Research Institute, SRM Institute of Science and Technology, SRM Nagar, Kattankulathur-603203, Chennai, Tamil Nadu, India

† Electronic supplementary information (ESI) available: Methods and materials, characterization methods and techniques, spectroscopic data of the obtained product and by-product, general reaction pathway for typical hydrogenation of cinnamaldehyde and applications of HCAL in different engineering aspects (Scheme S1), (a) synthesis of ZrO₂ support by a hydrothermal synthesis method and (b) synthesis of Pd@ZrO₂ catalysts by a wet-impregnation method (Scheme S2), (a) general illustration of depth analysis of XPS and TEM/EDX for elemental analysis and (b) TEM/EDX results obtained at the centre of the particle and at the edge of the particle of 4-Pd@ZrO₂ catalyst (Scheme S3), and comparative study of catalytic hydrogenation of cinnamaldehyde over 4-Pd@ZrO₂ with the literature (Table S1). See DOI: 10.1039/d0nj05595f

of both C=C and C=O).¹ All of these products have their own importance and applications in commercial sectors.^{1,2} The final product, HCOL, can be obtained irrespective of the type of catalyst employed in the cinnamaldehyde hydrogenation reaction. However, the challenge lies in designing a suitable catalytic system to selectively hydrogenate the C=C or C=O bond of CAL to obtain HCOL or COL, respectively.³ The emphasis herein lies in selectively yielding HCOL as it forms an important class of molecules having considerable industrial relevance.² The general reaction pathway followed by the hydrogenation of cinnamaldehyde in combination with certain industrial applications of HCOL is represented in Scheme S1 (ESI†).

With regards to this, literature studies reveal that versatile catalytic systems have been explored which involve the participation of active metals in combination with surface-modified supports.^{3,6} There are catalysts based on transition metals, noble metals, as well as the combination of both, which are supported on various supports such as CeO₂, CNT, graphene, SiO₂ and TiO₂ for the hydrogenation of cinnamaldehyde. Researchers have mainly worked on the surface modification of these catalysts to chemoselectively obtain cinnamyl alcohol or hydrocinnamaldehyde as a product.^{3,5,6} Various transition-metal-based catalysts such as Ni, Co, and Cu with suitable supports have been employed in the hydrogenation of cinnamaldehyde.⁶ These catalysts with certain surface modifications were found to be highly active in the hydrogenation of the C=O group of CAL to yield COL.^{2,3,5} Moreover, noble-metal-based catalysts such as Pt, Pd, Rh, and Au with appropriate surface modifications have also proven to be highly active towards the hydrogenation of the C=O group of CAL to yield COL.^{2,6-9} There are limited studies that have selectively obtained HCOL as the major product by employing hybrid catalysts such as Au-Cu, Pt-Ni, Pd-Ni, and Ni-Ir.^{1,6,10-13} Altogether, these literature studies reflect that, hydrogenation of C=C is favoured over the C=O bond as it is thermodynamically and kinetically stable.^{1,2} Also, noble-metal-based catalysts have been reported to yield COL.⁴ It is difficult to achieve controlled hydrogenation of C=C without affecting C=O over a noble-metal-based catalyst without making use of any poisons.⁴ Most of the available studies on the selective production of HCOL over noble metals have encountered moderate activities at relatively higher pressure, as not much focus has been devoted towards the surface modification of supports that can alter the physical and chemical properties of the active metal in the catalyst to favour the formation of HCOL.^{2,4} Among various noble metals, palladium (Pd) is considered as an appropriate candidate that can hydrogenate C=C present in conjugation with C=O.^{1,6} However, most of the reported Pd-based catalysts displayed moderate catalytic performance towards CAL to HCOL. It was found that a suitable support with surface modification is desirable to tune and control its electronic properties to achieve selectivity towards saturated aldehydes.^{1,6,9}

Among various support materials that have been widely studied, ZrO₂ was found to be an efficient candidate due to its moderate surface area, and high thermal stability and conductivity.^{9,14} ZrO₂ is known to behave as an inert support in the hydrogenation reactions.^{9,14} With suitable surface

modification, ZrO₂ can also act as an active metal and directly participates in the hydrogenation reactions.^{9,14} One of the strategies to modify the surface properties of ZrO₂ is to create oxygen vacancies which are related to the existence of surface Zr^{(4-x)+} sub-oxides.^{15,16} Literature studies clearly manifest that oxygen vacancies can be generated either by introducing dopant (La, Mg, Pd and Mn) or by reducing support in the presence of H₂.^{15,16} The latter one is quite difficult as ZrO₂ falls under the category of non-reducible oxides and requires high temperature and pressure.^{15,16} This is true for ZrO₂ bulk oxides and not for the smaller crystallites.^{15,16} There are also findings on the reduction of ZrO₂ and the resulting oxygen-vacancy creation by heating ZrO₂ in the presence of water.¹⁵ This procedure is believed to promote the formation of unstable surface -OH groups which further leads to the formation of oxygen defects.¹⁵ Accordingly, a lot of research has been done to synthesize oxygen-vacancy-rich nano-structured ZrO₂ which can be reduced at lower temperature and pressure to bring about constructive changes in the physical and chemical properties of ZrO₂ oxide.^{15,16}

With relevance to the above context, the present work features an oxygen-vacancy-rich Pd@ZrO₂ catalyst that offers certain prominent merits in comparison with the reported works. Precisely, the oxygen vacancies were developed in the ZrO₂ support of the Pd@ZrO₂ catalyst by a simple, low-temperature-assisted synthetic method. The synthesized oxygen-vacancy-rich Pd@ZrO₂ catalyst was characterized using various analytical, spectroscopic and microscopic techniques. The XPS and TEM analyses endorsed the successful formation of a nano-sized Pd@ZrO₂ catalyst with sufficient oxygen vacancies. The catalytic performance of the Pd@ZrO₂ catalyst towards the chemoselective hydrogenation of cinnamaldehyde was then investigated. The highly controlled nature of the 4-Pd@ZrO₂ catalyst led to 100% conversion of CAL with 86% yield towards HCOL at low H₂ pressure (10 bar) in comparison with the literature studies. We have also put in efforts to demonstrate the effects of varying temperature, pressure, active metal loading, catalyst loading and different solvents on the conversion and selectivity of the 4-Pd@ZrO₂-catalysed hydrogenation of cinnamaldehyde. All the conclusions drawn from the catalytic activities have been very well correlated with the characterization results. Additionally, a plausible mechanism has been constructed keeping in mind the role of oxygen vacancies, ZrO₂ surface modification and Pd active metal towards the chemoselective hydrogenation of cinnamaldehyde. The recyclability studies performed with the 4-Pd@ZrO₂ catalyst demonstrated consistency in the catalytic activity for six recycles without disturbing the physicochemical properties of the catalyst. However, in the present work, the authors have developed a noble-metal-based Pd@ZrO₂ catalyst for CAL hydrogenation. Taking into consideration the cost of noble metals, the authors will attempt in further work to replace the noble-metal-based catalysts with the cost-effective non-noble-metal-based catalysts for CAL hydrogenation. However, they strongly believe that the present work offers considerable advantages in comparison with other reported studies.

2. Experimental section

2.1. Synthesis of ZrO₂ support and impregnation of Pd over the as-synthesized ZrO₂ support

Zirconia (ZrO₂) was synthesized using the hydrothermal synthesis method reported elsewhere.¹⁶ Precisely, 10 mL of 0.5 M ZrO(NO₃)₂ solution was added to 60 mL of ethylene glycol under continuous stirring for around 15 min. Furthermore, the mixture was transferred into a 100 mL Teflon-lined autoclave which was tightly sealed and then heated at 180 °C for 16 h. After completion of the reaction, the autoclave was cooled to room temperature (30 °C) naturally. The obtained brown precipitate was collected and alternatively washed using DI water and ethanol by centrifuging at 4000 rpm for 5 min several times and dried at 60 °C for 6 h. Subsequently, the obtained material was annealed at 450 °C for 3 h at a ramping rate of 4 °C min⁻¹ to remove all the organic debris and produce ZrO₂ support.

Furthermore, Pd as the active metal was supported on ZrO₂ by a standard wet impregnation method.¹⁷ In particular, a certain amount (based on the wt% of Pd to be loaded on the ZrO₂ support) of palladium salt (Pd(NO₃)₂·2H₂O) was dissolved in 60 mL of DI water and accordingly, the appropriate amount of synthesized ZrO₂ support was then introduced into the aqueous solution of Pd precursor under vigorous stirring to ensure homogeneous dispersion of Pd metal onto the ZrO₂ support matrix. The entire solution was kept under stirring at 90 °C until all the water evaporated and a complete dry powder residue was left over. The resultant powder was then calcined at 450 °C for 3 h at a ramping rate of 4 °C min⁻¹ to obtain the desired catalyst in its oxide form which is henceforth designated as PdO@ZrO₂. Prior to use in the reaction, the catalyst was freshly reduced in a H₂ atmosphere at a flow rate of 30 mL min⁻¹ at 100 °C for 3 h, which was the actual catalyst hereafter designated as Pd@ZrO₂. Various Pd@ZrO₂ catalysts with different Pd loading were also synthesized in a similar manner by using appropriate quantities of Pd precursor. The final catalysts thus obtained are designated as 1-Pd@ZrO₂, 2-Pd@ZrO₂, 3-Pd@ZrO₂, 4-Pd@ZrO₂, 5-Pd@ZrO₂ and 6-Pd@ZrO₂, respectively, wherein the numerical values denote the amount of Pd loading in wt%. The entire synthesis procedure for the Pd@ZrO₂ catalysts is represented in Scheme S2 (ESI[†]).

2.2. Selective hydrogenation of cinnamaldehyde (CAL) over Pd@ZrO₂ catalysts

The catalytic activity of Pd@ZrO₂ catalysts towards the selective hydrogenation of CAL was performed in an indigenous 100 mL stainless-steel high-pressure reactor coupled with a magnetic stirrer and an automated temperature controller. Typically, an appropriate amount of pre-reduced catalyst (at 100 °C for 3 h) was transferred into the autoclave without exposing it to the atmosphere. The reactor was then charged with the reactant cinnamaldehyde (CAL, 1 g) and 10 mL of a suitable solvent. The reactor was sealed tightly and the system was purged with pure H₂ gas three times to ensure the complete removal of residual air and finally, the system was pressurized to the desired

pressure with H₂ gas. The gas was continuously passed into the system and the H₂ pressure was maintained with a pressure controller. The reaction was initiated by stirring at a speed of 600 rpm to neglect the external mass transfer limitation and the system was heated to the required temperature. Zero reaction time was noted as soon as the system was placed in the heating unit. The hydrogenation reaction was allowed to run for the desired time period and the temperature, pressure and agitation speed were maintained at constant values throughout the reaction cycle. After completion of the reaction, the H₂ gas inlet was closed following which stirring and heating were switched off. The reactor was allowed to cool to room temperature naturally. Then, the system was slowly depressurized by releasing excess hydrogen. The reaction mixture was filtered using Whatman filter paper to separate the catalyst. The reaction progress and the product formation for the Pd@ZrO₂-catalyzed hydrogenation of CAL were monitored and confirmed by analyzing the reaction mixture and the authentic samples of reactant as well as products using a gas chromatograph (GC-7820 A; M/S Agilent, USA) equipped with a flame ionization detector (FID) having a capillary column (HP-5, 19091J-413) of 30 m length, 0.32 mm inner diameter and 0.25 mm film thickness. The products from the reaction mixture were separated by HPLC technique and the obtained products, HCOL (major) and HCOL (minor), were confirmed by ¹H NMR and ¹³C NMR spectroscopic techniques and GC-MS as well as elemental analysis.

Spectral data of the major product, *hydrocinnamaldehyde* (HCAL) [*3-phenylpropanal*] (*conversion-100%*, *selectivity-86%*, *yield-86%*): According to the general procedure, the separated compound, HCAL, was obtained as a colorless liquid; b.p. 97–98 °C;

¹H NMR (400 MHz, CDCl₃): δ (ppm) = 9.810 (t, 1H), 7.32 (t, 2H), 7.24–7.19 (m, 3H), 2.89 (t, 2H), 2.69 (s, 2H). ¹³C NMR (100 MHz, CDCl₃) δ 201.32, 140.48, 128.48, 128.28, 126.18, 45, 28.11; HRMS calculated for C₉H₁₀O [M + H]⁺: 134.07; found: 135.08; elemental analysis: C, 80.54; H, 7.52; O, 11.93.

Spectral data of the minor product, *hydrocinnamyl alcohol* (HCOL) [*3-phenylpropanol*] (*conversion-100%*, *selectivity-14%*, *yield-14%*): According to the general procedure, the separated compound, HCOL, was obtained as a pale yellow liquid; b.p. ~235 °C;

¹H NMR (400 MHz, CDCl₃): δ (ppm) = 7.31 (t, 2H), 7.25–7.18 (m, 3H), 3.50 (t, 2H), 1.81 (m, 2H), 2.63 (t, 2H), 1.71 (s, 1H). ¹³C NMR (100 MHz, CDCl₃) δ 140.89, 128.41, 128.41, 125.81, 128.42, 128.41, 32.11, 34.21, 61.59; HRMS calculated for C₉H₁₂O [M + H]⁺: 136.09; found: 137.0987; elemental analysis: C, 79.35; H, 8.89; O, 11.76.

3. Results and discussion

As discussed, Pd was loaded on ZrO₂ supports to generate and enhance oxygen vacancies which are believed to alter the electronic properties of Pd that might be responsible for the chemoselective nature of Pd@ZrO₂ catalysts.¹³ Based on this

conceptual strategy, it is necessary to provide appropriate evidence for the successful synthesis of ZrO_2 supports and Pd@ZrO_2 catalysts with different Pd loading. Thus, the materials were characterized by various advanced analytical, spectroscopic and microscopic techniques to determine their phases as well as analyze their morphological and physicochemical properties. These results may perhaps provide an understanding of the characteristics of Pd@ZrO_2 catalysts that could aid in the chemoselective hydrogenation of cinnamaldehyde to hydrocinnamaldehyde.

3.1. Catalyst characterization

3.1.1. XRD analysis. XRD analysis was performed to obtain information on the crystallinity and phase purity of the as-synthesized materials.¹⁸ Fig. 1(a) shows the XRD patterns of the ZrO_2 support and the Pd@ZrO_2 catalysts with different Pd loading. It is well reported that pure ZrO_2 can occur in either of the three phases: monoclinic, tetragonal or cubic, or it can exist as a mixed phase.¹⁹ The existence of different phases in ZrO_2 is strongly dependent on the procedure followed during the synthesis.²⁰ The XRD patterns of the ZrO_2 support synthesized by the solvothermal synthesis method in the present work displayed sharp diffraction peaks that emphasize the crystalline nature of the support. The peaks positioned at 30.2° , 35.1° , 50.6° , 60.1° , 63.0° and 74.7° in the XRD patterns of the ZrO_2 support correspond to the respective [101], [110], [112], [211] and [220] planes. These planes are in good correlation with the characteristic peaks of ZrO_2 with a pure tetragonal phase and well match the International Center for Diffraction Data (ICDD) file no. 80-0965.²⁰ The average crystallite size (D) of the tetragonal ZrO_2 nanoparticles was calculated for the dominant tetragonal diffraction peak at [101] using the Debye Scherrer formula and was found to be around 10.2 nm.²⁰

Similarly, the XRD analysis of the various Pd@ZrO_2 catalysts with different Pd loading was also performed after freshly reducing the catalysts in the H_2 atmosphere at 100°C for 3 h. The XRD patterns of various Pd@ZrO_2 catalysts with Pd loading displayed in Fig. 1(a) show the diffraction peaks corresponding to the tetragonal phase of the ZrO_2 support according to the ICDD file no. 80-0965.²⁰ Additionally, three peaks were also observed at 2θ values of $\sim 40.3^\circ$, 46.75° and 65.94°

corresponding to the [111], [200] and [220] planes, respectively.²¹ This exemplifies the presence of Pd with a face-centered cubic crystal structure (ICDD file no. 05-0681).²¹ Furthermore, a short, low-intensity diffraction peak observed at a 2θ value of $\sim 38.6^\circ$ infers the presence of PdO.²² This could possibly be due to the oxidation of Pd to PdO upon exposure to an air atmosphere during analysis. Additionally, the peaks centered at 2θ values of $\sim 28.2^\circ$, 32.2° and 56° were also detected which correspond to $[-111]$, [111] and [130] diffraction planes, respectively.²⁰ These characteristic diffraction peaks belong to the monoclinic phase of the ZrO_2 support which correlates with the ICDD file no. 37-1484.²⁰ This implies that a certain percentage of the pure tetragonal phase in the ZrO_2 support has been transformed into the monoclinic phase during the Pd impregnation process.²³ The cause for this transition at moderately low temperatures ($65\text{--}400^\circ\text{C}$) can be attributed to the presence of chemisorbed water molecules on the oxygen vacancies of the ZrO_2 lattice initiated as an aqueous Pd precursor solution employed during the Pd impregnation process.²³ This is in good agreement with the mechanism anticipated for this transition by Guo *et al.*^{23,24} This transformation initiated due to Pd impregnation is supposed to stabilize the tetragonal phase of the ZrO_2 support in the Pd@ZrO_2 catalyst.²⁵ The percentage composition of tetragonal and monoclinic phases in various Pd@ZrO_2 catalysts with different Pd loading was estimated with the help of the Rietveld method.¹⁵ The calculated parameters are listed and summarized in Fig. 1(b). The obtained XRD results revealed that the percentage of the tetragonal phase was observed to decrease with the increase in the Pd loading. Additionally, a slight shift was observed in the position of all the peaks that could possibly be due to the presence of lattice defects and hence the occurrence of zirconium in sub-oxide forms.

Subsequently, the crystallite size of various Pd@ZrO_2 catalysts with different Pd loading was calculated for the intense peak at [111] using the Debye Scherrer formula.²⁰ The calculated data displayed in Fig. 1(b) clearly show that there is an increase in the crystallite size of the Pd@ZrO_2 catalysts with an increase in Pd loading. With the increase in Pd loading, there could be a possibility of agglomeration of the Pd nanoparticles on the ZrO_2 support which resulted in an

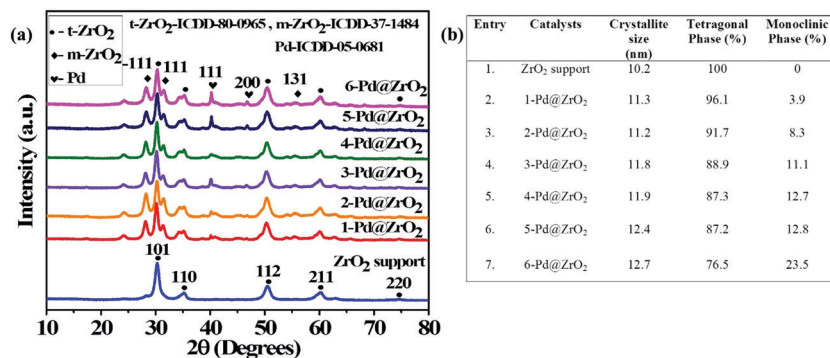


Fig. 1 (a) XRD patterns of ZrO_2 support and Pd@ZrO_2 catalysts with different wt% Pd loading (where t- ZrO_2 corresponds to tetragonal ZrO_2 , and m- ZrO_2 corresponds to monoclinic ZrO_2) and (b) summary of crystallite size and calculated phase content.

increase in the crystallite size of the Pd@ZrO₂ catalysts.²⁶ This increasing trend in the crystallite size with respect to the increase in the Pd loading is clearly observed in Fig. 1(b).

3.1.2. FE-SEM analysis. In order to obtain insight into the morphology, the molecular surface structures of as-synthesized materials were characterized using a field-emission scanning electron microscopy (FE-SEM) technique.¹⁸ ZrO₂ supports, as well as various Pd@ZrO₂ catalysts with different Pd loading, were analyzed at various magnifications, the FE-SEM results of which are shown in Fig. 2. The FE-SEM images of ZrO₂ support shown in Fig. 2(a) consist of a rod-like morphology. We presume that the ZrO₂ nanoparticles synthesized in the presence of ethylene glycol under solvothermal conditions led to the formation of rod-like nanostructures having average uniform length and thickness. According to one of the reports by Sahar and Masoud, ethylene glycol which is widely used as a

solvent plays a dual role of behaving as a complexing as well as a capping agent in the synthesis of nanoparticles.²⁷ Ethylene glycol as a complexing agent has a tendency to produce homometallic and heterometallic glycolates by alcoholysis of ligands existing in the metal precursors.²⁸ In the present study, zirconium nitrate in the presence of ethylene glycol underwent pre-alcoholysis and resulted in the formation of zirconium glycolate which precipitated out from the solution due to its lower solubility.²⁸ A continuous increase of the zirconium glycolate (monomer) concentration led to the beginning of the crystallization process.²⁹ This step is in accordance with the theory proposed by La Mer *et al.*²⁹ Once the concentration crossed the saturation limit, fast busting of nucleation began which produced zirconium glycolate nuclei in large numbers.²⁹ The surface area kept on increasing due to the newly formed nuclei.²⁹ To compensate for this, a reduction in bulk surface energy occurred by forming new crystal lattices.²⁹ This eventually led to a reduction in the Gibbs energy which turned out to be a reason for the continuous growth.²⁹ The zirconium glycolate nuclei grew large at the cost of the zirconium glycolate monomer until its concentration dropped below the saturation level.²⁹

The final shape of the zirconium glycolate particles will be determined by the surface energies of the planes.²⁹ The planes in the crystal with higher surface energy will grow more rapidly to stabilize and lower its surface energy.²⁹ The ethylene glycol bound strongly to a specific plane with higher surface energy which lowered the surface energy of that plane and facilitated the growth of zirconium glycolate along a one-dimensional direction resulting in a rod-like morphology.²⁹ Finally, the calcination of zirconium glycolate led to the formation of a ZrO₂ support with a rod-like morphology, the surface of which appeared to be smooth throughout the analysis, which could specifically be observed at a higher magnification of 100 nm as shown in Fig. 2(a).

The FE-SEM analysis was also performed for all the various Pd@ZrO₂ catalysts with different Pd loading. The results for all Pd@ZrO₂ catalysts are displayed in Fig. 2(b-g). Initially, with 1-Pd@ZrO₂, 2-Pd@ZrO₂ and 3-Pd@ZrO₂ catalysts, we could observe a rod-like structure and the surface appeared smooth. However, on observing the FE-SEM images of 4-Pd@ZrO₂, 5-Pd@ZrO₂ and 6-Pd@ZrO₂ catalysts, the surface of the Pd@ZrO₂ appeared to be rough and cracked in comparison with the surface of the ZrO₂ support. The tetragonal phase of ZrO₂ becomes unstable due to the presence of chemisorbed water molecules on the oxygen vacancies of the ZrO₂ lattice initiated during the Pd impregnation process. Thus, some parts of the unstable tetragonal phase may get transformed into a monoclinic phase during the calcination process of the PdO@ZrO₂ precursor in order to reduce the stress and stabilize the tetragonal phase of ZrO₂. This transformation of phase may lead to the development of cracks on the surface of the catalyst.³⁰ The FE-SEM results undoubtedly portrayed retention in the surface morphology for all Pd@ZrO₂ catalysts with different Pd loading. However, with the increase in the Pd loading, there was a gradual increase in the transformation of the tetragonal phase into a monoclinic phase. The presence of

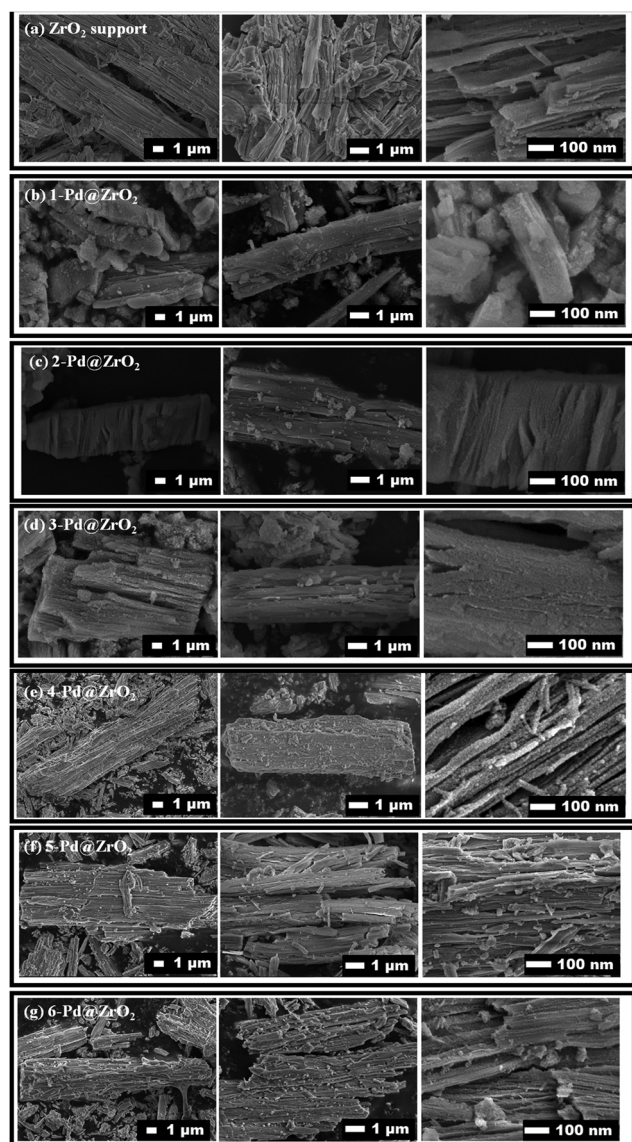


Fig. 2 FE-SEM analysis of (a) the ZrO₂ support and (b-g) various Pd@ZrO₂ catalysts with different Pd loading.

the monoclinic phase along with the tetragonal phase in the Pd@ZrO₂ catalysts with different wt% Pd loading can be well-corroborated with the results obtained in the XRD analysis.

The elemental composition of the synthesized ZrO₂ support and the various Pd@ZrO₂ catalysts with different Pd loading was quantitatively analyzed using EDX and elemental mapping analysis and the results are shown in Fig. 3(a–g) and the inset of Fig. 3(a–g), respectively. The EDX graph of the ZrO₂ support showed the presence of only Zr and O elements which signifies that the ZrO₂ support has been successfully synthesized with high purity. Additionally, the elemental mapping shown in the

inset of Fig. 3(a) confirms the even distribution of the Zr and O elements on the surface of the ZrO₂ support. Similarly, the elemental analysis of the various Pd@ZrO₂ catalysts with different Pd loading was also performed which is shown in Fig. 3(b–g). The EDX graphs of 1-Pd@ZrO₂, 2-Pd@ZrO₂ and 3-Pd@ZrO₂ catalysts displayed the presence of Zr, O and Pd elements in agreement with their respective stoichiometry. Similarly, the expected stoichiometry of Zr, Pd and O was also observed in 4-Pd@ZrO₂, 5-Pd@ZrO₂ and 6-Pd@ZrO₂ catalysts. The presence of the expected elements confirmed the successful impregnation of Pd on the ZrO₂ support. Moreover, the

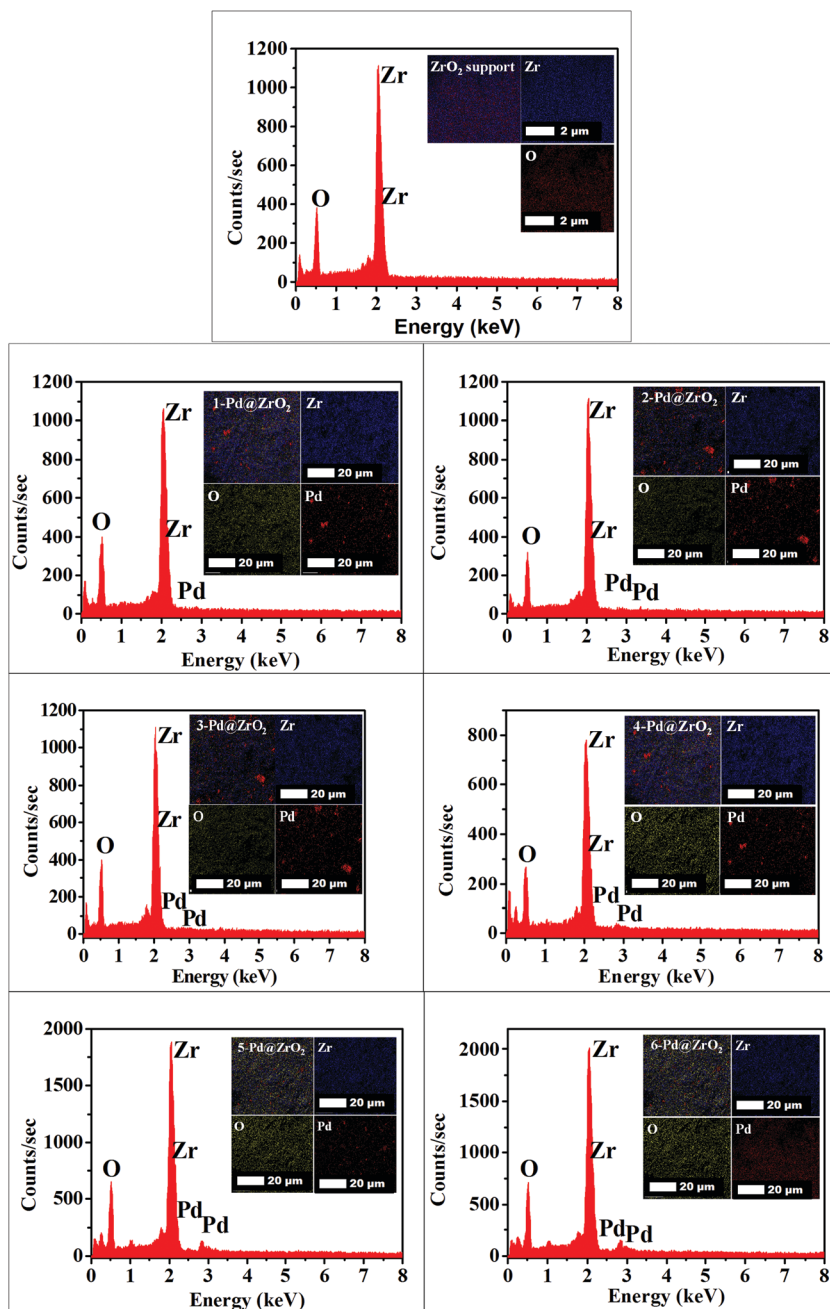


Fig. 3 EDX analysis of (a) ZrO₂ support and (b–g) various Pd@ZrO₂ catalysts with different Pd loading and the elemental mapping of (inset of a) ZrO₂ support and (inset of b–g) various Pd@ZrO₂ catalysts with different Pd loading.

elemental mapping shown in the inset of Fig. 3(b–g) further elucidated the uniform dispersion of all the elements on the surface of the various Pd@ZrO₂ catalysts with different Pd loading.

3.1.3. TEM and HR-TEM analyses. Controlled experiments discussed in the initial activity studies revealed that the 4-Pd@ZrO₂ catalyst displayed outstanding results and hence TEM and XPS analyses were performed only for the 4-Pd@ZrO₂ catalyst in order to evaluate the presence and enhancement of oxygen vacancies. TEM and HR-TEM techniques are very crucial in understanding the catalyst morphology, assessment of size and particle size distribution of nanoparticles and determination of lattice fringes.²⁸ Due to this, the ZrO₂ support and 4-Pd@ZrO₂ catalyst were analyzed using TEM and HR-TEM and the results are displayed in Fig. 4. The TEM image of the ZrO₂ support shown in Fig. 4(A-1) clearly displayed a rod-like morphology which is in good accordance with the morphology obtained through the FE-SEM analysis. The particle size distribution plot revealed that the average particle size of the ZrO₂ support is 9.5 nm which is in good agreement with the ZrO₂ crystallite size calculated from the XRD analysis. The histogram of particle size distribution showed that the size of the ZrO₂ nanoparticles ranged from 8 to 14 nm with an average particle size of 9.5 nm. This value is in good agreement with the crystallite size value calculated using the Debye-Scherrer equation.

The high-resolution TEM image of the ZrO₂ support illustrated in Fig. 4(B-1) commonly showed a lattice spacing of 0.3 nm, which resembles the [101] plane of the tetragonal

ZrO₂.^{20,31,32} Additionally, lattice fringes with 0.27 nm spacing were also found which correspond to the [110] plane of the tetragonal ZrO₂.^{20,33} Thus, the HR-TEM analysis confirmed the predominant presence of the tetragonal phase in the ZrO₂ support. This discussion is in line with that of the XRD data wherein the dominant diffraction peak of the tetragonal ZrO₂ relates to the [101] plane. SAED patterns were also acquired for the tetragonal ZrO₂ which displayed the presence of small spots making up the concentric rings, a characteristic pattern observed for polycrystalline materials.³⁴ Each concentric ring corresponds to the diffraction plane which is identified by measuring the distance between two bright spots in each ring and is shown in Fig. 4(C-1). The above elucidation is in correlation with the literature.³⁴

The TEM image of the ZrO₂ support in the 4-Pd@ZrO₂ catalyst shown in Fig. 4(A-2) signifies the presence of larger crystallites as compared to the ZrO₂ support with a pure tetragonal phase. Its corresponding histogram of particle size distribution showed the presence of particles of sizes ranging from 8 to 16 nm with an average particle size of 10.5 nm. This value also correlates with the crystallite size calculated using the XRD data. The HR-TEM and SAED analyses were also performed for the 4-Pd@ZrO₂ catalyst which resulted in the patterns shown in Fig. 4(B-2,3) and (C-2,3), respectively. The inter-planar d-spacing was calculated which showed the presence of the monoclinic phase along with the tetragonal phase. The d-spacing of 0.28 nm and 0.34 nm corresponds to the [111] and [110] planes of the monoclinic phase of the ZrO₂

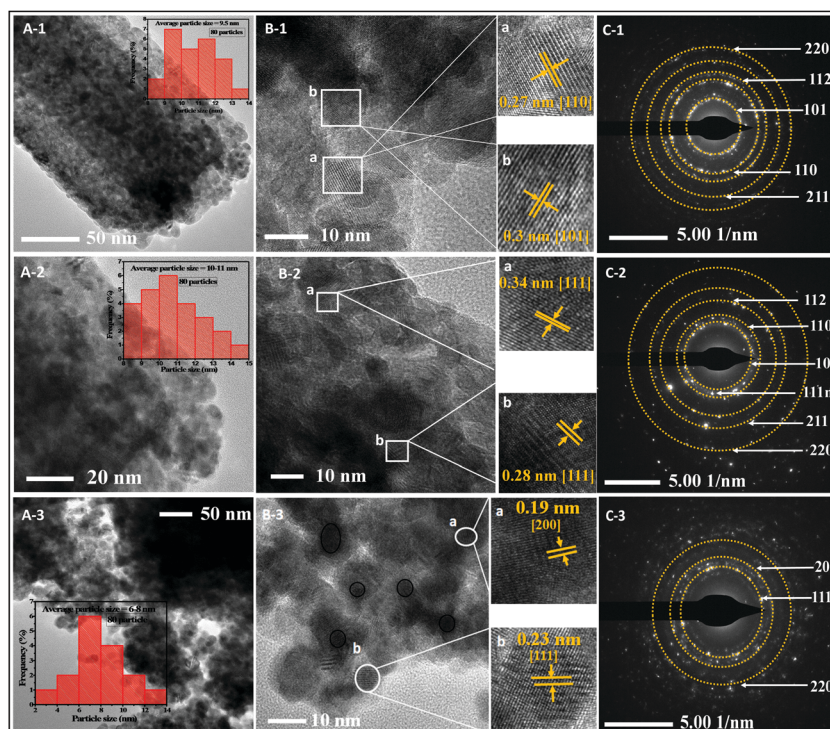


Fig. 4 TEM analysis of (A-1) the ZrO₂ support, (A-2) ZrO₂ in the 4-Pd@ZrO₂ catalyst and (A-3) Pd in the 4-Pd@ZrO₂ catalyst; HR-TEM analysis of (B-1) the ZrO₂ support, (B-2) ZrO₂ in the 4-Pd@ZrO₂ catalyst and (B-3) Pd in the 4-Pd@ZrO₂ catalyst; and SAED patterns of (C-1) the ZrO₂ support, (C-2) ZrO₂ in the 4-Pd@ZrO₂ catalyst and (C-3) Pd in the 4-Pd@ZrO₂ catalyst.

support.^{20,34–37} The presence of ZrO₂ as a mixed phase (tetragonal + monoclinic) in the 4-Pd@ZrO₂ catalyst has also been confirmed by the XRD analysis. The SAED patterns show diffraction spots forming concentric rings each of which is indexed to the respective planes as shown in Fig. 4(C-2). There is an occurrence of a diffraction spot relating to the [111] plane of the monoclinic phase which additionally supports the presence of the monoclinic phase in the 4-Pd@ZrO₂ catalyst.³⁸

The TEM image of Pd in the 4-Pd@ZrO₂ catalyst is also displayed in Fig. 4(A-3) which demonstrated a spherical-shaped Pd over the ZrO₂ support. The corresponding histogram of particle size distribution showed the presence of Pd particles with sizes ranging from 2 to 14 nm with an average particle size of 7 nm. The inter-planar d-spacing of 0.23 nm and 0.19 nm was obtained as shown in Fig. 4(B-3) which could be related to the respective [111] and [200] planes of the face-centered cubic Pd nanoparticles.^{39,40} The SAED patterns displayed concentric rings which confirm the polycrystalline nature of the material.⁴¹ The concentric ring corresponding to the respective planes of Pd is displayed in Fig. 4(C-3) which can also be correlated with the XRD analysis. The TEM-EDX analysis was also performed for both the ZrO₂ support and the 4-Pd@ZrO₂ catalyst which confirmed the presence of the respective elements in the material. The TEM-EDX analysis was helpful in the indirect assessment of oxygen vacancies in the material and hence it has been discussed in brief in Section 3.2.

3.1.4. XPS analysis. The hydrogenation reaction is a surface phenomenon and thus it is important to understand the surface chemistry of the catalytic material.¹⁷ The XPS technique is considered as an effective tool for the surface analysis of the material to obtain detailed information on its elemental composition, chemical state, as well as the electronic state.¹⁸ Both the ZrO₂ support and the 4-Pd@ZrO₂ catalyst were subjected to XPS analysis. Survey spectra, spectra for Zr 3d, O 1s and C 1s, were obtained for the ZrO₂ support. The survey spectra confirmed the presence of the required components in the ZrO₂ support. The obtained spectra were deconvoluted and the peak fitting was performed using CASA XPS software.⁴² The survey spectra and all the deconvoluted graphs are displayed in Fig. 5(a–d). The XPS spectra of Zr 3d showed four peaks after deconvolution which could be related to the presence of Zr in different oxidation states.⁴³ Various literature reports suggest that the binding energy for Zr3d_{3/2} and Zr3d_{5/2} occurs at 182.0 and 184.4 eV, respectively.²⁰ However, in the present study, two peaks for Zr 3d_{3/2} and Zr 3d_{5/2} were observed at the binding energy of 184.5 and 186.9 eV, respectively. The binding energy for the Zr 3d peak was observed to be shifted to a higher binding energy which could possibly be due to the presence of oxygen vacancies.⁴⁴ The difference in the binding energy was 2.4 eV which confirmed the presence of Zr⁺⁴ species.²⁰ This is in accordance with the literature.^{20,45} The shoulder peak observed at the base of Zr 3d_{3/2} with a binding energy of 182.7 eV could be ascribed to oxygen deficiency which could be because of the under-coordinated Zr sites in the ZrO₂ support.⁴⁴ An additional peak at a low binding energy of 180.5 eV corresponds to the

presence of Zr^{(4-x)+} ions.⁴⁴ Literature reports articulate that the electrons present in the lattice after the formation of oxygen vacancies could possibly be utilized in the reduction of nearby Zr⁺⁴ ions and this probably could be the reason for the presence of Zr^{(4-x)+} species.⁴⁶ The O 1s spectra with a single peak after deconvolution displayed three peaks corresponding to the presence of three different oxygen species.⁴⁴ A peak centered at 530.4 eV corresponds to the presence of lattice oxygen.⁴⁶ A peak at 528.3 eV represents the presence of chemisorbed oxygen (OH⁻) species and a peak at 532.5 eV could be related to low coordinated oxygen species (O⁻¹).⁴⁶ The interpretation of O 1s deconvoluted spectra is significant to understand and clarify the concept of oxygen vacancies and thus it is discussed separately in Section 3.2. Finally, the carbon peak C 1s could be ascribed to some residual carbon detected from the sample or the hydrocarbon from the XPS instrument itself.⁴⁷

Furthermore, the XPS analysis of the 4-Pd@ZrO₂ catalyst was also studied in detail and the obtained survey spectra, spectra for Pd 3d, Zr 3d, C 1s and O 1s and their respective deconvoluted spectra, are represented in Fig. 5(e–j). The survey spectrum indicated the presence of Pd, Zr, O and C elements. The deconvoluted spectrum of Pd 3d showed two peaks centered at 333.20 eV and 346.6 eV which corresponds to Pd 3d_{3/2} and Pd 3d_{5/2}, respectively.⁴⁸ These peaks can be assigned to the presence of Pd.⁴⁸ Furthermore, as the literature reports indicated that the Zr 3p₃ peak overlaps the Pd 3d_{5/2}, the Zr 3p₃ peak was also deconvoluted which is shown as two peaks.⁴⁸ A low-intensity shoulder peak obtained after the deconvolution of Zr 3p₃ peak at 336.9 eV is attributed to the presence of Pd⁺² which could be due to the oxidation of Pd to PdO due to the exposure of the catalyst to the atmosphere during analysis.⁴⁸ The deconvoluted Zr 3d spectra showed four peaks similar to that of the ZrO₂ support. However, a slight shift in the binding energy was observed which could be due to the increase in the defect concentration.⁴⁴ The peaks at 182.53 eV and 184.93 eV could be assigned to Zr 3d_{3/2} and Zr 3d_{5/2}, respectively.⁴⁴ The difference in the binding energy of these two peaks was found to be 2.4 eV which yet again confirmed the presence of Zr⁺⁴ species which is consistent with the literature.¹⁶ The low binding energy peak centered at 180.23 eV corresponds to the presence of Zr^{(4-x)+} ions.⁴³ The shoulder peak is observed at the base of Zr 3d_{3/2} with a binding energy of 182.7 eV which is characterized for the presence of oxygen deficiency due to the under-coordinated Zr sites in the material.⁴⁴ The deconvoluted O 1s spectra displayed three peaks evincing the presence of three different oxygen species the same as in the case of the ZrO₂ support. The detailed analysis is discussed in Section 3.2.

3.1.5. BET surface area and pore size distribution analysis. The specific surface area of the as-synthesized ZrO₂ support and the various Pd@ZrO₂ catalysts with different Pd loading was evaluated precisely by BET analysis by employing a nitrogen adsorption–desorption technique at liquid N₂ temperature (–77 K). Prior to the analysis, the materials were degassed at 100 °C for 3 h in order to remove all adsorbed water and other gases from the surface of the material. The BET plots obtained by employing this technique provided useful information on the

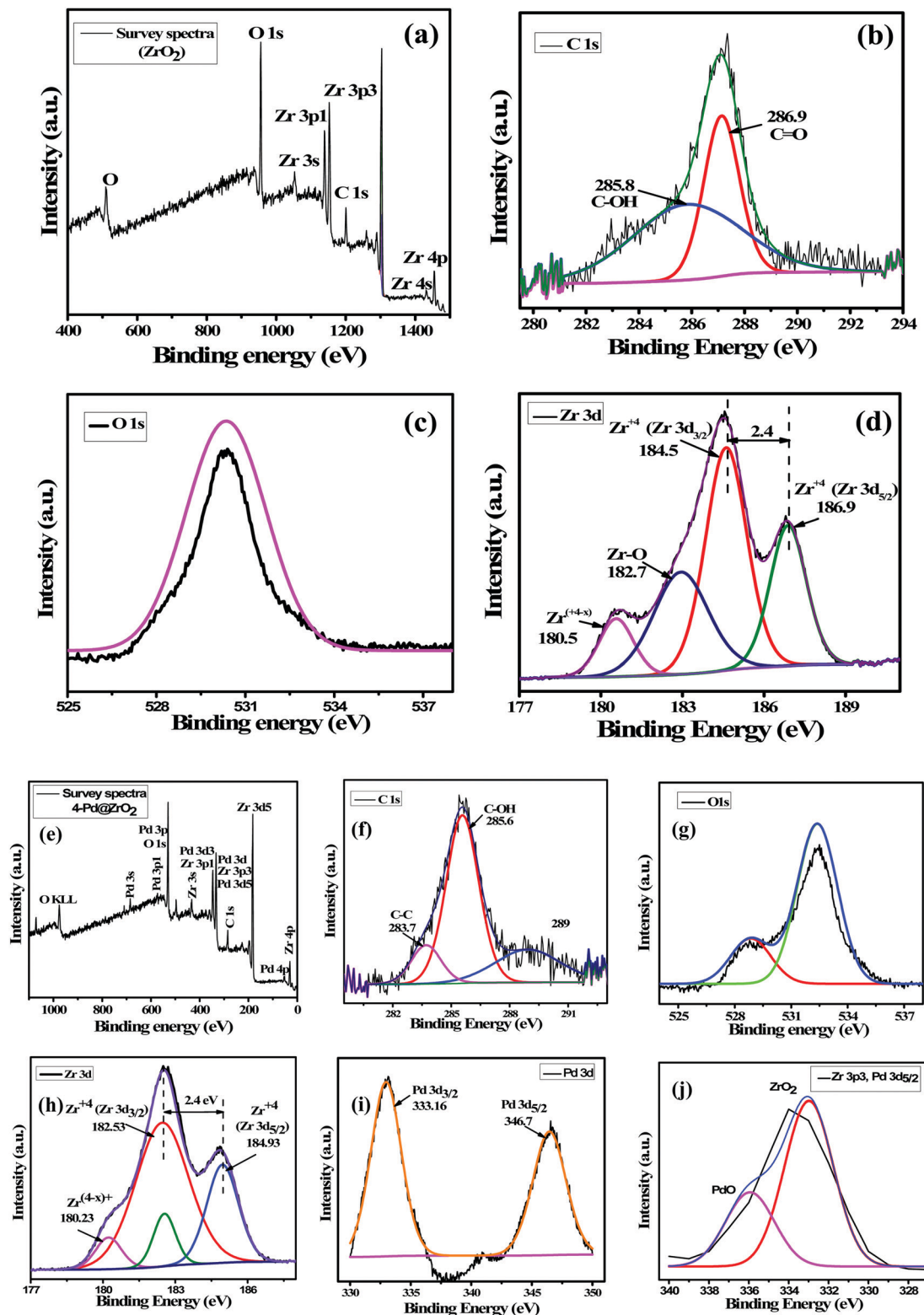


Fig. 5 XPS of ZrO_2 support: (a) survey spectra, (b) C 1s spectra, (c) O 1s spectra and (d) Zr 3d spectra; XPS of the 4-Pd@ ZrO_2 catalyst: (e) survey spectra, (f) C 1s spectra, (g) O 1s spectra, (h) Zr 3d spectra, (i) Pd 3d spectra and (j) Zr 3p3 spectra.

surface porosity and pore diameter of the materials.²⁰ Fig. 6(a and b) represent the respective BET and BJH plots of the ZrO_2 support and the various Pd@ ZrO_2 catalysts with

different Pd loading. The specific surface area of the ZrO_2 support was found to be around $37 \text{ m}^2 \text{ g}^{-1}$. The graph displayed a type IV isotherm with H1 hysteresis loop which is a typical

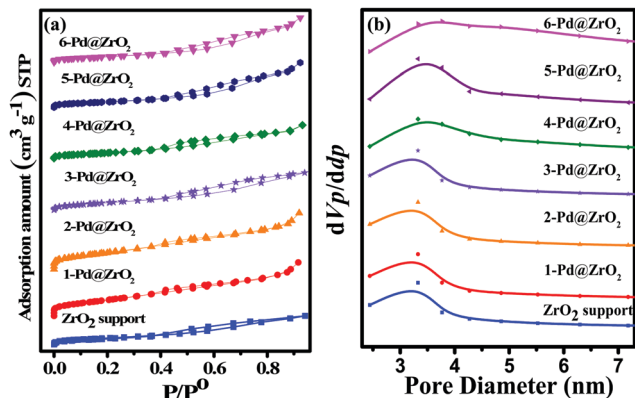


Fig. 6 BET plots of (a) ZrO_2 support and various Pd@ZrO_2 catalysts with different Pd loading and BJH plots of (b) ZrO_2 support and various Pd@ZrO_2 catalysts with different Pd loading.

characteristic of mesoporous materials.⁴⁹ Hence, it can be said that the ZrO_2 support is porous in nature and can be utilized as a good support material which is also supported by one of the reports by Deshmane *et al.*¹⁴

The specific surface area of the various Pd@ZrO_2 catalysts with different Pd loading was also estimated and the obtained results are summarized in Table 1. All the graphs reflected a type IV isotherm with H1 hysteresis loop similar to that of the ZrO_2 support. The impregnation of Pd on the ZrO_2 support possibly introduced additional pores leading to the development in the porosity of the final Pd@ZrO_2 catalyst. The increase in the pore volume for 1 wt% Pd@ZrO_2 in comparison with that of the ZrO_2 support complements the results obtained and supports the discussion. A similar trend in the results has also been observed in the literature.^{50–53} With further increase in Pd loading (2, 3, 4, 5 and 6 wt%), the surface area gradually decreased. In agreement with the decrease in the surface area, the pore volume was also observed to decrease. It is known that with a larger crystallite size, the surface area tends to lower down.⁵³ Hence, a decrease in the specific surface area with respect to the increasing Pd loading can also be correlated with the crystallite size of the catalysts as calculated using the [111] plane of the XRD diffractogram. Moreover, an increase in the Pd loading from 2 wt% to 6 wt% might have led to agglomeration

Table 1 Textural properties of ZrO_2 support and various Pd@ZrO_2 catalysts with different Pd loading

Entry	Catalysts	BET surface area ^a ($\text{m}^2 \text{g}^{-1}$)	Pore volume ^a ($\text{cm}^3 \text{g}^{-1}$)	Pore diameter ^a (nm)	Acidity ^b ($\mu\text{mol g}^{-1}$)
1.	ZrO_2 support	36.6	0.059	3.33	0.52
2.	1-Pd@ ZrO_2	82.7	0.094	3.35	1.0
3.	2-Pd@ ZrO_2	85.6	0.097	3.38	4.2
4.	3-Pd@ ZrO_2	75.6	0.094	3.42	6.6
5.	4-Pd@ ZrO_2	44.1	0.076	3.52	8.6
6.	5-Pd@ ZrO_2	38.3	0.066	3.54	12.6
7.	6-Pd@ ZrO_2	36.0	0.063	3.55	18.4

^a Calculated from BET. ^b Calculated from NH_3 -TPD analysis from the summation of areas under the peaks.

and thus blockage of pores with Pd particles, and these could also be the reasons for the decrease in the surface area of the catalysts with increasing Pd loading as supported by the literature.²⁶

The pore size distribution and pore diameter of the ZrO_2 support and the various Pd@ZrO_2 catalysts with different Pd loading were acquired by employing the BJH method. The mean pore diameter calculated for the ZrO_2 support and the various Pd@ZrO_2 catalysts with different Pd loading is displayed in Table 1, which confirms the mesoporous nature of these materials. Furthermore, the ZrO_2 support and various Pd@ZrO_2 catalysts with different Pd loading showed an increase in pore diameter with an increase in Pd loading.

3.1.6. H_2 -TPR and NH_3 -TPD analyses. Various Pd@ZrO_2 catalysts with different Pd loading were analyzed using H_2 -temperature programmed reduction (TPR) in order to determine the most effective reduction condition to reduce PdO to active Pd⁰.²³ This technique could provide information on the extent of the interaction of the Pd metal with the ZrO_2 support.¹⁸ H_2 -TPR profiles of the ZrO_2 support and various Pd@ZrO_2 catalysts with different Pd loading are shown in Fig. 7(a). The H_2 -TPR profile of the ZrO_2 support synthesized in the present work displayed a single, broad peak centered at 581 °C which is ascribed to the reduction of ZrO_2 .⁵⁴ Various literature reports articulate that it is difficult to reduce pure ZrO_2 nanocrystals and the tentative reduction temperature of Zr^{+4} is above 500 °C.⁵⁴ The H_2 -TPR profile of the 1-Pd@ ZrO_2 catalyst suggests the presence of an intense peak at a lower temperature of 94 °C which is attributed to the reduction of superficial PdO present on the catalyst surface.^{55,56} A minor broad peak at 362 °C corresponds to the reduction of the PdO present on the catalyst surface in the bulk phase.⁵⁷ One broad peak at a higher temperature of 628 °C was also evidenced which might be due to the reduction of ZrO_2 present at the metal-support interface.⁵⁴ Similar kinds of H_2 -TPR profiles were observed for the 2-Pd@ ZrO_2 , 3-Pd@ ZrO_2 and 4-Pd@ ZrO_2 catalysts. In the H_2 -TPR profile of most of the reported Pd-based catalyst systems, a negative peak in the temperature range of 50 °C to 120 °C is usually detected which indicates the presence of β -Pd-hydride. The β -Pd-hydride species is formed due to the decomposition of the weakly adsorbed hydrogen from the Pd surface at room temperature. The presence of this negative peak corresponding to β -Pd-hydride indicates the existence of larger Pd particles on the catalyst surface.^{56,58} However, the peak in this region was not observed in the reduction profiles of the Pd@ZrO_2 catalysts till 4 wt% Pd loading which suggests the presence of nano-sized Pd particles in these catalysts.⁵⁹ These results are well supported by the data obtained from the XRD and BET analyses.

Surprisingly, a negative peak corresponding to β -Pd-hydride was observed in the H_2 -TPR profiles of the 5-Pd@ ZrO_2 and 6-Pd@ ZrO_2 catalysts at 120 °C.^{56,58} The appearance of this negative peak infers the presence of larger PdO particles in the 5 wt% and 6 wt% Pd-loaded Pd@ZrO_2 catalysts.^{56,58} Additionally, peaks resulting from the reduction of bulk PdO and ZrO_2 were observed at 383 °C and 598 °C, respectively.^{54,57}

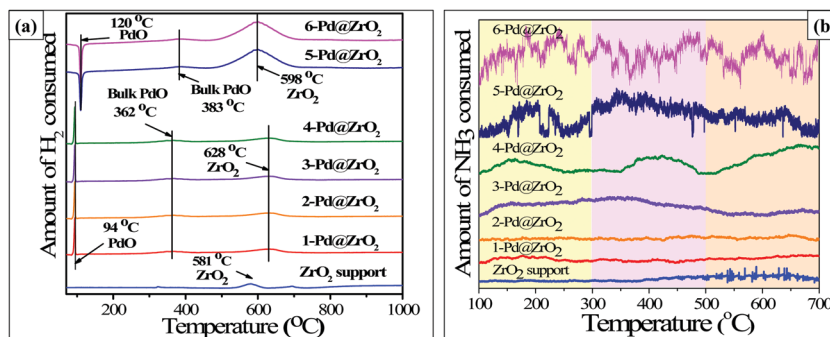


Fig. 7 (a) H₂-TPR profiles of ZrO₂ support and various Pd@ZrO₂ catalysts with different Pd loading and (b) NH₃-TPD profiles of ZrO₂ support and various Pd@ZrO₂ catalysts with different Pd loading.

The presence of larger Pd crystallites in the 5-Pd@ZrO₂ and 6-Pd@ZrO₂ catalysts is also evidenced by the XRD data represented in Table 1. The above discussion is in alignment with the reported literature.^{56–58} Based on the H₂-TPR analysis, 100 °C was chosen as the reduction temperature for the various Pd@ZrO₂ catalysts with different Pd loading to preferably reduce PdO into Pd⁰ and activate the Pd@ZrO₂ catalysts.

Moreover, the extent of the acidic and basic sites on the surface of the metal oxides is essentially important in order to understand and predict the performance of a catalyst in the hydrogenation reactions.⁶⁰ The surface acidity of the Pd@ZrO₂ catalysts was quantified by TPD analysis employing NH₃ gas as a probe molecule.⁶⁰ The NH₃-TPD profiles of the ZrO₂ support as well as the various Pd@ZrO₂ catalysts with different Pd loading are displayed in Fig. 7(b). Before the interpretation of graphs, it is necessary to understand the classification of acidic sites on the basis of the desorption of basic NH₃ molecules with respect to the change in the temperature.⁶¹ Peaks observed below 300 °C correspond to the weak acidic sites, whereas the desorption of NH₃ molecules from moderate acidic sites occurs between 300 °C and 450 °C and strong acid sites adsorbed NH₃ that are released above 450 °C.⁶¹

Taking this into consideration, the NH₃-TPD graphs of all the materials were elucidated. The graph of the ZrO₂ support showed the presence of one small peak in the region below 300 °C which corresponds to the presence of weak acidic sites.⁶⁰ Furthermore, two small peaks in the region between 300 °C and 450 °C were observed at 325 °C and 410 °C, respectively.⁶⁰ These peaks were obtained due to the desorption of the weakly bonded NH₃ molecules by hydrogen bonding which corresponds to the moderate acidic sites and not due to the desorption of ammonia from the surface of the acidic sites of the ZrO₂ support.⁶⁰ The total acidity of the ZrO₂ support calculated by measuring the area of the ammonia desorption peaks was calculated to be 0.516 μmol g⁻¹ which suggested that the ZrO₂ support has a very low acidic nature.

Similarly, the various Pd@ZrO₂ catalysts with different Pd loading were also analyzed using NH₃-TPD for quantifying the presence of acidic sites and the results are displayed in Fig. 7(b). The obtained result reveals the presence of three broad and intense peaks respectively, in all three regions of the

various Pd@ZrO₂ catalysts with different Pd loading.⁶² Precisely, a peak centered at 198 °C corresponds to the presence of weak acidic sites obtained from the desorption of hydrogen-bonded NH₃.⁶² This particular peak can also be attributed to the presence of Brønsted acidic sites (Zr-OH) as the bonding between NH₃ and Brønsted acid sites is weaker and can easily be broken down at lower temperatures.⁶² The appearance of a peak at 415 °C confirmed the presence of moderately acidic sites.⁶² Finally, a peak centered at 680 °C relates to the presence of strong acidic sites.⁶² With respect to the increase in the Pd loading, the number of acidic sites was also observed to increase. A similar result for the increase in acidity with respect to the increase in the Pd loading has also been reported by Srinivas *et al.*⁶³ The conclusion can be drawn from the above discussion that, impregnation of Pd on the ZrO₂ support drastically enhanced the acidic character of the Pd@ZrO₂ catalysts with different Pd loading which is essentially an important factor to trigger the hydrogenation reaction in the forward direction.⁶¹

3.1.7. H₂-chemisorption studies. Chemisorption techniques have been widely employed with H₂ as a probe molecule, especially for Pd-based catalysts.⁶³ This technique assists to gain information on the number of accessible active sites, the surface area of active sites, the metal particle size and also the percent metal dispersion, prominently for noble-metal-based heterogeneous catalysts.¹⁸ Thus, to acquire all this information for the various Pd@ZrO₂ catalysts with different Pd loading, the materials were subjected to H₂ chemisorption analysis and the results calculated are presented in Table 2.

As could be observed, an increase in the Pd loading notably affected the Pd particle size as well as the extent of Pd dispersion. With the increase in the Pd loading, a gradual decrease in the metal dispersion was evidenced which might possibly be due to agglomeration.⁵² This trend can also be evidenced in the present case wherein, the increase in Pd loading from 1 wt% to 6 wt% decreased the metal dispersion with a comparative increase in the Pd particle size. This trend is in good correlation with the literature.²⁶ The increase in the Pd particle size with the increase in the Pd loading should undoubtedly lead to a decrease in the surface area of the catalysts.²⁶ This observation is in line with the BET analysis

Table 2 H₂-chemisorption measurements for various Pd@ZrO₂ catalysts with different Pd loading

Entry	Catalysts	Pd particle size (nm)	Pd metal dispersion (%)	Pd metal surface area (m ² g ⁻¹)	H ₂ uptake (mmol g ⁻¹)
1	1-Pd@ZrO ₂	1.27	89	392	0.2
2	2-Pd@ZrO ₂	1.32	86	380	0.4
3	3-Pd@ZrO ₂	1.33	82	376	0.6
4	4-Pd@ZrO ₂	1.49	72	335	0.7
5	5-Pd@ZrO ₂	2.18	50	229	0.6
6	6-Pd@ZrO ₂	3.13	35	160	0.5

wherein the surface area was observed to decrease with the increase in Pd content (Table 1).

3.1.8. FT-IR spectroscopic studies. FT-IR analysis was performed to confirm the existence of the metal oxide framework and different functional groups in the synthesized materials.⁴⁵ Fig. 8 represents the FT-IR spectrum of the ZrO₂ support which displays a broad peak at 3396 cm⁻¹ that corresponds to the -OH stretching vibration from the surface hydroxyl groups.⁶⁴ Additionally, a peak at 1635 cm⁻¹ and 1385 cm⁻¹ can be attributed to the bending vibrations of -OH and vibrations due to the non-bridging -OH groups, respectively.⁶² The presence of peaks at 658 and 582 cm⁻¹ is due to the vibrations of the tetragonal Zr-O bond as also confirmed in one of the reports by Jayakumar *et al.*⁶⁴ In the FT-IR spectrum of the various Pd@ZrO₂ catalysts with different Pd loading, similar parent peaks corresponding to the presence of the ZrO₂ support were evidenced. Additionally, a peak observed at 740 cm⁻¹ corresponded to the vibration of m-ZrO₂.⁴⁵ Moreover, we also observed the characteristic peaks in the fingerprint region between 700 cm⁻¹ and 450 cm⁻¹ which confirmed the presence of the M-O framework.⁶⁵ The spectra obtained for all the Pd@ZrO₂ catalysts were similar to each other with regularity

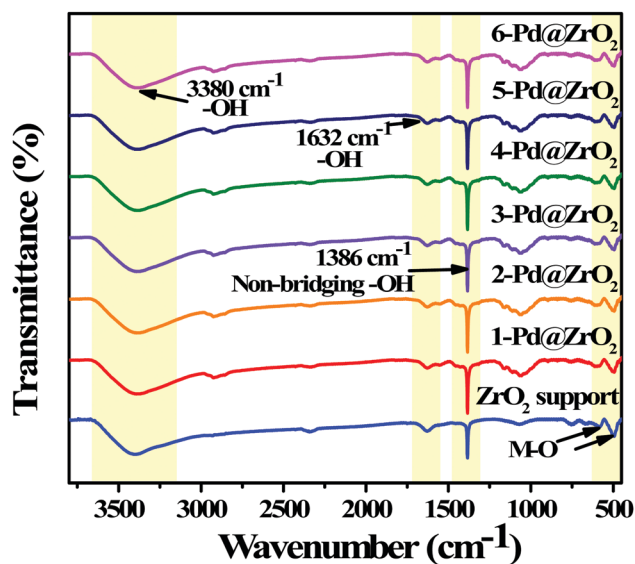


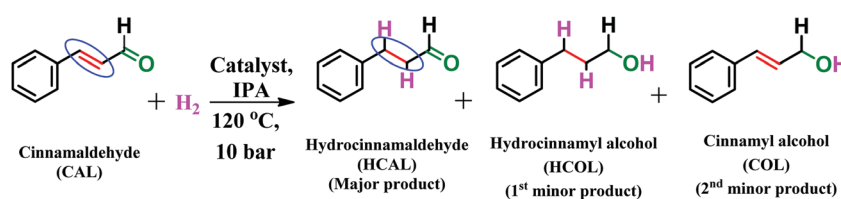
Fig. 8 FT-IR spectra of ZrO₂ support and various Pd@ZrO₂ catalysts with different Pd loading.

in peak positions as can be seen in Fig. S4 (ESI[†]). This interpretation correlates with that in one of the literature studies by D'souza *et al.*⁶⁵

3.1.9. Catalytic activity screening of the CAL hydrogenation reaction with the prepared Pd@ZrO₂ catalysts. After confirming the successful synthesis of oxygen-vacancy-rich Pd@ZrO₂ catalysts by employing various spectroscopic and analytical techniques, the catalysts were tested for their activity and selectivity towards the hydrogenation of cinnamaldehyde. Initially, certain controlled experiments were performed in order to get insight into the behavior of Pd@ZrO₂ catalysts for the selective hydrogenation of cinnamaldehyde. The outcome of the reactions performed is tabulated in Table 3. To begin with, the cinnamaldehyde (CAL) hydrogenation reaction was screened in the absence of a catalyst and solvent at 120 °C and 10 bar H₂ pressure (Table 3, entry 1). Insignificant conversion and selectivity towards hydrocinnamaldehyde (HCAL) were evidenced. However, good selectivity was obtained towards hydrocinnamyl alcohol (HCOL; a complete hydrogenated product) which is supposed to form regardless of the type of catalyst or reaction parameters employed for the reaction.⁶⁶ This reaction demonstrated that in the absence of both the catalyst and the solvent, the reaction did not run and these two parameters are immensely important to selectively drive the reaction and avoid the formation of the completely hydrogenated product (HCOL). Furthermore, with the aim to investigate the impact of varying the Pd loading on the selective hydrogenation of CAL, the reactions were performed by charging 1 g CAL, using 10 mL IPA, loading different wt% Pd on Pd@ZrO₂ at 120 °C, and using 10 bar H₂ pressure for a time period of 9 h.

Preliminarily, with 1 wt% Pd@ZrO₂ catalysts, a noteworthy conversion of 95.1% was observed which accentuated that Pd in its zero oxidation state acts as an active metal and has a tendency to readily dissociate molecular hydrogen and adsorb onto its surface (Table 3, entry 2). This phenomenon has a vital impact on the conversion of CAL. However, the selectivity of only 60.3% and 30.7% towards HCAL and HCOL, respectively, could be achieved with 1 wt% Pd@ZrO₂ catalysts. The remaining 9% selectivity was accredited to COL. Performing reactions with 2 wt% Pd@ZrO₂ catalysts did not bring much alteration in the conversion (98.8%) and selectivity (63.5%) towards HCAL (Table 3, entry 3). The remaining two products, HCOL and COL, were also obtained in 32.5% and 4% selectivity, respectively. On the other hand, by employing 3 wt% Pd@ZrO₂ catalysts, an increase in the selectivity towards the desired product HCAL (72.0%) was observed with a conversion of 95.6% (Table 3, entry 4). The selectivity of the remaining two products was reduced to 25.4% and 2.6%, respectively. Availability of more dispersed active sites on the catalyst surface could have led to the increase in the selectivity of the desired product which has been confirmed by the H₂ chemisorption studies.

Furthermore, 100% conversion was achieved with 4 wt% Pd@ZrO₂ catalysts with 86% selectivity towards HCAL (Table 3, entry 5). The only by-product obtained using the 4-Pd@ZrO₂ catalyst was HCOL with 14% selectivity. This trend suggested

Table 3 Catalytic activity screening of the CAL hydrogenation reaction with the prepared Pd@ZrO₂ catalysts^a


Entry	Reaction parameters	Conversion (%)	Selectivity (%)		Yield (%) HCAL ^b
			HCAL	HCOL	
1	Solvent and catalyst free	5	3.2	60	0.2
2	1-Pd@ZrO ₂	95.1	60.3	30.7	59.2
3	2-Pd@ZrO ₂	98.7	63.5	32.5	63
4	3-Pd@ZrO ₂	95.6	72	25.4	69
5	4-Pd@ZrO ₂	100	86	14	86
6	5-Pd@ZrO ₂	100	67.1	27.9	67.1
7	6-Pd@ZrO ₂	100	47	24	47
8	With ZrO ₂	19.3	96.4	3.6	18.6
9	With PdO	68	36	42	24.5
10	With Pd ⁰	95	50.6	30	48.0
11	Catalyst free, with IPA solvent	14.9	65	35	2.9
12	With catalyst, IPA solvent free	97.9	40.8	21	39.9
13	N ₂ atmosphere (10 bar)	2.5	3	35	0.1
14	Atm. Pressure (H ₂)	86.7	1.9	5.8	1.7
15	At R.T.	15	10	18	15

^a Reaction conditions: 4-Pd@ZrO₂, 1g CAL, 10 mL IPA, 10 bar H₂, temperature, and 9 h. ^b Calculated using GC.

that Pd as an active metal played a major role in enhancing the conversion of CAL. Also, Pd in association with ZrO₂ support gradually improved the selectivity and hence the yield of HCAL. Additionally, reactions with 5 and 6 wt% Pd@ZrO₂ catalysts were also performed in an attempt to obtain higher yields. Nevertheless, a drop in the selectivity towards HCAL was observed though there was consistency in the conversion of almost 100%. With 5 wt% Pd@ZrO₂ catalysts, 67.1% selectivity was achieved for HCAL (Table 3, entry 6). HCOL and COL were obtained in 27.9% and 5% selectivity, respectively. With 6 wt% Pd@ZrO₂ catalysts, selectivity for HCAL dropped to 47%. HCOL and COL were obtained in 24% and 29% selectivity, respectively (Table 3, entry 7). From this particular discussion, it could be inferred that 4 wt% Pd@ZrO₂ catalysts could possibly provide enough active sites for complete conversion of CAL. Furthermore, an increase in the Pd loading decreased the selectivity and increased the formation of HCOL. The excess of active sites present in the 5-Pd@ZrO₂ and 6-Pd@ZrO₂ catalysts led to the further hydrogenation of HCAL which resulted in the formation of the complete hydrogenated product HCOL and a marginal amount of COL was also detected.⁶⁶ Additionally, the high acidic nature of the catalysts with 5 and 6 wt% Pd loading can also be one of the reasons for the formation of the by-products (Table 1).⁶⁶ Furthermore, the unsatisfying results obtained using 5-Pd@ZrO₂ and 6-Pd@ZrO₂ as the catalysts could also be due to the agglomerated Pd particles on the ZrO₂ support as a result of less dispersion as supported by the H₂ chemisorption data. Overall, the literature shows the same trend and thus supports the conclusion drawn from the effects of the Pd loading study.¹²

From these initial screenings, it was clear that the 4-Pd@ZrO₂ catalyst in the presence of IPA solvent led to high conversion and

selectivity towards HCAL. Furthermore, reactions were also performed in the presence of ZrO₂ support which showed low conversion and low yield towards HCAL (Table 3, entry 8). Furthermore, to investigate whether the hydrogenation of cinnamaldehyde proceeds in the presence of Pd⁺² or metallic Pd, the reaction was performed in the presence of PdO as well as metallic Pd and the results were compared. In the presence of PdO catalyst (Pd in +2 state), 68% conversion and 36% selectivity were observed which were unexpectedly pretty good results (Table 3, entry 9). It is known that PdO is much less capable of adsorbing and thus dissociated the molecular hydrogen into atomic hydrogen which can then be utilized in the hydrogenation of the reactant. However, in the present scenario, there can be a possibility of *in situ* reductions of PdO during the reaction course as the reaction was performed at 120 °C by supplying H₂ externally. This could be the reason for achieving the high conversion of CAL over PdO as a catalyst. When the reaction was performed in the presence of metallic Pd, 95% conversion was achieved by selectively yielding 50.6% HCAL (Table 3, entry 10). The results obtained confirmed that the high hydrogenating capacity of Pd as an active metal in its zero state is responsible for achieving the high conversion of CAL. However, in the absence of ZrO₂ support, the achieved selectivity was comparatively low. These outcomes convincingly illustrate that both the active metal Pd and the ZrO₂ support act synergistically for achieving high conversion and selectivity towards HCAL.

Furthermore, few reactions were also performed to reveal the individual role of the solvent and catalyst in the selective hydrogenation of CAL. The reaction performed in the presence of a solvent and the absence of a catalyst showed only 14.9% conversion which indicated that the solvent could not bring

about effective conversion single-handedly. However, moderate selectivity of 65% was observed for HCAL which showed the probable role of a solvent in obtaining selectivity (Table 3, entry 11). On performing the reaction with a catalyst and without a solvent, the conversion of around 98% was observed which represents the intrinsic role of the presence of a catalyst in the reaction (Table 3, entry 12). Additionally, selectivity of 40.8% was observed for HCAL which is lower than that observed in the previous reaction in the presence of a solvent. All these observations may possibly suggest that the catalyst is solely responsible for achieving the conversion in the presence of H_2 . It is worth highlighting that 100% conversion and 86% selectivity were obtained towards HCAL in the presence of the 4-Pd@ZrO₂ catalyst and IPA solvent (Table 3, entry 5). The result thus illustrates that both the catalyst and the solvent are responsible for obtaining HCAL with high selectivity.

The 4-Pd@ZrO₂ catalyst along with the IPA solvent is believed to enhance the selectivity towards HCAL as evidenced from the above reactions. However, IPA is also known to act as a hydrogen donor in the transfer hydrogenation process.⁶⁷ Hence, a reaction was performed without supplying H_2 externally under the following reaction conditions: 4-Pd@ZrO₂, 1g CAL, 10 mL IPA, 10 bar N₂, 120 °C and 9 h reaction time to confirm the role of IPA in the present reaction. Low CAL conversion of 2.5% and HCAL selectivity of 3% were obtained in an N₂ atmosphere which emphasized that IPA was not capable of providing hydrogen for the conversion of CAL (Table 3, entry 13).⁶⁷ This experiment indicated that IPA did not play the role of hydrogen donor but only behaved as a solvent in the 4-Pd@ZrO₂-catalyzed CAL hydrogenation. Few controlled experiments were performed to also investigate the role of pressure and temperature in the CAL hydrogenation over the 4-Pd@ZrO₂ catalyst. Under atmospheric pressure, the appreciable conversion was observed; however, negligible selectivity of 2% towards HCAL was evidenced (Table 3, entry 14). On performing the reaction at room temperature, both conversion and selectivity were observed to be lower than 15% (Table 3, entry 15). These two reactions demonstrated the importance of pressure and temperature, respectively. Taking all these controlled experiments into consideration, several activity studies were performed with respect to the 4-Pd@ZrO₂ catalyst loading, reaction time, and

effects of different solvents followed by the effects of temperature and pressure on the CAL hydrogenation over the 4-Pd@ZrO₂ catalyst which has been discussed further in detail. From the above experiments, it is clear that the CAL hydrogenation performed over the 4-Pd@ZrO₂ catalyst generated three products: hydrocinnamaldehyde (HCAL) as the major product, and hydrocinnamyl alcohol (HCOL) and cinnamyl alcohol as minor products which were confirmed by GC as well as GC-MS analyses. Hereafter, the selectivity of HCAL and HCOL will be taken into account. It is to be noted that the remaining minor percentage of selectivity is for COL.

3.2. Evaluation of oxygen vacancy enhancement in the 4-Pd@ZrO₂ catalyst

As the physicochemical properties of the metal oxides could be improved by the presence of oxygen vacancies, it is thus very important to directly or indirectly investigate the oxygen vacancies using various spectroscopic and microscopic techniques.¹³ Therefore, a careful evaluation of the presence of oxygen vacancies in the ZrO₂ support and its enhancement in the 4-Pd@ZrO₂ catalyst was carried out to support the concept of oxygen vacancies controlling the selectivity of HCAL in the CAL hydrogenation. For this, XPS, FE-SEM-EDX and TEM-EDX analyses quantitatively provided useful information. In XPS, deconvoluted O 1s spectra of the ZrO₂ support displayed three peaks as shown in Fig. 9(a), wherein a peak centered at 530.4 eV corresponds to the presence of lattice oxygen.⁴⁶ A peak at 528.3 eV represents the presence of chemisorbed oxygen (OH⁻) species.⁴⁶ The peaks at higher binding energy (531–532 eV) correspond to the weakly adsorbed oxygen species on the surface of the material.⁴⁶ Ionization of these weakly adsorbed oxygen species could permit compensation for some defects in the subsurface of the metal oxides which can be referred to as low coordinated oxygen ions (O¹⁻).⁴⁶

Precisely, a peak at 532.5 eV indirectly indicates the presence of oxygen vacancies as it is reported that the concentration of adsorbed oxygen species is related to the presence of oxygen vacancies.⁴⁶ The percentage concentration of oxygen vacancies in the ZrO₂ support has been calculated by integrating the peak area using CASA XPS which showed the presence of 9.3% of oxygen defects in the ZrO₂ support. A similar analysis performed for the 4-Pd@ZrO₂ catalyst conveyed that the

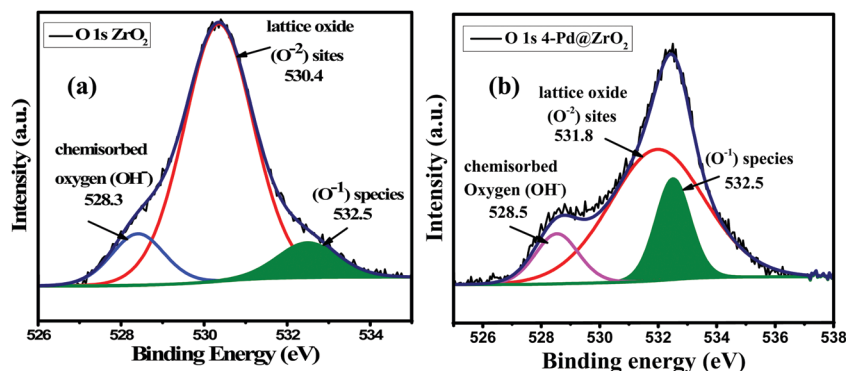


Fig. 9 Deconvoluted spectra of O 1s (a) for ZrO₂ support and (b) 4-Pd@ZrO₂ catalyst.

intensity of a peak at the binding energy of 531.8 eV for the lattice oxygen (O^{2-}) was observed to decrease as compared to that for the ZrO_2 support. In line with this, the intensity of a peak centered at 532.5 eV increased which could be related to the increase in the oxygen vacancies as can be seen in Fig. 9(b). The percentage concentration of oxygen vacancies calculated for 4-Pd@ ZrO_2 by integrating the peak area using CASA XPS software was found to be 18.4% which is higher than that for the ZrO_2 support. Moreover, the electrons generated during oxygen-vacancy creation could possibly be used to reduce the Zr^{4+} to its sub-oxides.⁴⁶ The deconvoluted spectrum of Zr 3d clearly depicts the presence of the sub-oxides of Zr^{4+} species.⁴⁶ Thus, the presence of $Zr^{(4-x)+}$ reduced species is also evidence for the existence of oxygen vacancies.⁴⁶ The percentage (%) concentration of $Zr^{(4-x)+}$ species was calculated for both the ZrO_2 support and the 4-Pd@ ZrO_2 catalyst which was found to be 6.5% and 9.5%, respectively, which again complements the oxygen-vacancy enhancement in the 4-Pd@ ZrO_2 catalyst. The XPS analysis thus illustrated that the oxygen-vacancy concentration is higher in the 4-Pd@ ZrO_2 catalyst than that in the ZrO_2 support which could help in enhancing the selectivity towards HCAL. The percentage composition of the respective elements and the binding energies of different oxygen species in the ZrO_2 support and 4-Pd@ ZrO_2 catalyst are presented in Table 4. The above discussion is very well supported by the literature.^{68–70}

Moreover, it is known that XPS analysis can be utilized to examine the surface stoichiometry of mainly a few atomic layers at the surface, say up to 5–10 nm in depth.⁷¹ In order to measure the bulk concentration of the elements in the material, say up to 100 nm, TEM-EDX analysis could be an appropriate spectroscopic technique.⁷² This complementary analysis can indirectly provide useful quantitative information on the presence of oxygen vacancies at the surface as well as in the bulk.^{72,73} The results obtained by the quantitative analyses of XPS and TEM-EDX are presented in Table 5. Precisely, the computable analysis was performed at the boundary and at the center part of the particle to determine the amount of oxygen species present and are shown in Table 5. It could be seen that the percentage of oxygen species at the boundary is less than that in the interior part. Additionally, the literature studies support the fact that the addition of metal leads to the formation of oxygen vacancies. In the present work, impregnation of Pd on the ZrO_2 support surface is believed to enhance oxygen vacancies

Table 4 Chemical composition of respective elements obtained by XPS analysis and the binding energies of different oxygen species in the ZrO_2 support and 4-Pd@ ZrO_2 catalyst

Samples	Chemical composition (%)			Binding energy (eV)		
	Zr	O	Pd	Lattice oxygen (O^{2-})	Chemisorbed oxygen (OH^-)	Low coordinated oxygen species (O^{-1})
ZrO_2 support	21.2	78.8	—	530.4	528.3	532.5
4-Pd@ ZrO_2	28.81	60.2	10.99	531.1	528.5	532.5

Table 5 The atomic percentage of respective elements obtained by XPS analysis and weight percentage of respective elements obtained by TEM analysis

Entry	Catalysts	Atomic% of elements			Wt% of elements	
		XPS			TEM (boundary)	TEM (center)
		Oxygen species	Zr ^{(4-x)+} species	Oxygen vacancies	Oxygen species	Oxygen species
1.	ZrO_2 support	78.8	6.5	9.3	55.3	62.3
2.	4-Pd@ ZrO_2 catalyst	60.2	9.4	18.4	45.3	52.0

in the ZrO_2 support at the surface. Thus, we observe less oxygen species at the boundaries as compared to those in the central bulk portion. Hence, we presume that the concept of calculating the amount of oxygen species from the XPS and TEM-EDX data and correlating them could be considered valid as the results are in line with each other. The idea behind this analysis is illustrated in Scheme S3 (ESI[†]).

3.3. Effects of various reaction parameters on the CAL hydrogenation reaction with Pd@ ZrO_2 catalysts

3.3.1. Effects of 4-Pd@ ZrO_2 catalyst loading on the CAL hydrogenation reaction. The activity of any catalytic reaction depends on the amount of active surface sites made available for the reaction.⁷⁴ Hence, it is mandatory to study the effects of the 4-Pd@ ZrO_2 catalyst loading on the hydrogenation of CAL. In this study, the reactions were performed by employing different wt% of the 4-Pd@ ZrO_2 catalyst under the same reaction conditions as above. The reaction results are compiled and shown in Fig. 10. To begin with, a neat reaction without catalyst under optimized reaction conditions of temperature (120 °C) and H_2 pressure (10 bar) could convert only 15% CAL with selectively producing 75% HCAL along with HCOL and COL as minor products. This signifies that the presence of a catalyst in the reaction is of utmost importance in order to bring out the effective conversion of CAL.⁶² On the introduction

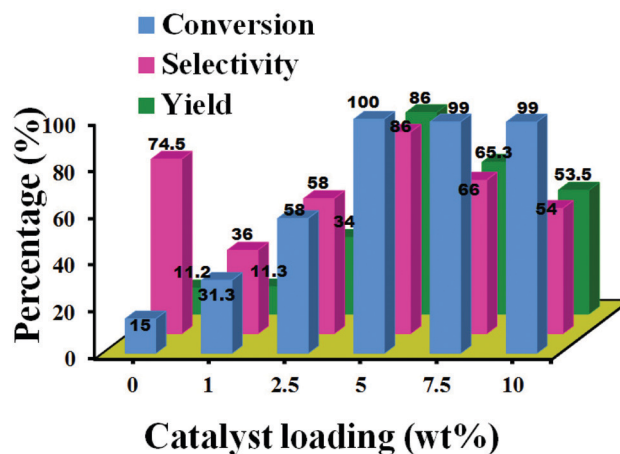


Fig. 10 Catalytic performance over different loading of the 4-Pd@ ZrO_2 catalyst.

of the 1 wt% 4-Pd@ZrO₂ catalyst in the reaction, a slight increase in the conversion (31.3%) was observed with 36% selectivity towards the major product HCAL. Introduction of the 1 wt% 4-Pd@ZrO₂ catalyst in the reaction did not provide sufficient catalytic sites for the reactants to react and therefore low conversion of CAL was obtained.⁷⁴

Increasing the catalyst loading to 2.5 wt% gradually increased the conversion and selectivity to 58% and 58%, respectively. Furthermore, an increase in catalyst loading was continued to 5 wt% which showed 100% conversion of CAL with 86% selectivity towards HCAL and the calculated yield was estimated to be 86% with only HCOL as the minor product. Although the desired conversion was achieved, to further study the effects of increasing the catalyst loading on selectivity, the reaction with 7.5 wt% and 10 wt% of catalyst loading was also performed. As expected, the conversion remained 100%; however, there was a drop in the selectivity for HCAL and an increase in the HCOL product formation with the presence of COL in minor quantities. The reason for this observation could be attributed to the presence of excess of active sites on the catalyst surface that might lead to further hydrogenation of HCAL to form the completely hydrogenated product HCOL.⁷⁴ The similar cause for the formation of HCOL is reported by Kluson *et al.*⁷⁴ The commendable activity observed with 5 wt% of the 4-Pd@ZrO₂ catalyst loading could be attributed to the presence and availability of sufficient active sites for the reactant to react.⁷⁴ The increase in the conversion of CAL up to 5 wt% loading suggests that the reaction follows first-order kinetics with respect to the catalyst loading. The trend observed in the catalyst loading study is also in accordance with the available literature.⁷⁴ In conclusion, the 5 wt% 4-Pd@ZrO₂ catalyst showed excellent conversion with 86% yield towards HCAL and thus was chosen as an optimized catalyst loading for further reactions.

3.3.2. Effects of reaction time on CAL hydrogenation reaction. In addition to catalyst loading, reaction time is also a crucial parameter to control the activity and selectivity of the Pd@ZrO₂ catalyst for the hydrogenation of CAL.⁷⁵ Hence, the reaction was performed by varying the reaction time and the results are displayed in Fig. 11. Initially, the reaction was conducted under optimized reaction conditions for an hour. The reaction proceeded with 99% conversion and 51.4% selectivity towards HCAL. Furthermore, with an increase in the reaction time to 3 h and then 9 h, the conversion remained the same. The selectivity of 54% was obtained at 3 as well as 6 h reaction time. When the reaction time was extended to 9 h, an increase in the selectivity was observed with an 86% yield of HCAL. Interestingly, the only by-product detected was HCOL along with the HCAL as the desired product. Furthermore, the reaction was run for 12 h in which a decrease in the selectivity towards HCAL was observed with a slight increase in the selectivity towards HCOL. This signifies that after 9 h of reaction time, HCAL produced during the reaction course further hydrogenated to form HCOL, thus decreasing the yield of HCAL.⁷⁵ It could be inferred from the above study that HCAL or COL could be produced from the hydrogenation of CAL.⁷⁵ Though, with progressing time, both

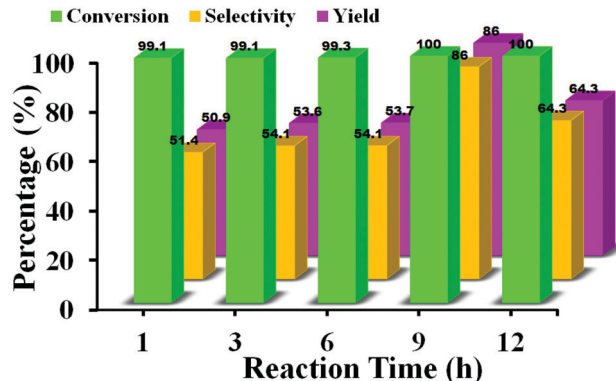


Fig. 11 Catalytic activity study over Pd@ZrO₂ catalyst with different reaction times (reaction conditions: 4-Pd@ZrO₂, 1g CAL, 10 mL solvent, 120 °C temperature, 10 bar H₂, and 9 h).

HCAL and COL are converted into HCOL, the rate of the latter getting converted into HCOL is greater.⁷⁵ Therefore, in a 9 h reaction time, HCAL was obtained selectively from CAL hydrogenation and COL produced in the reaction was completely converted into HCOL. Hence, 9 h was fixed as an optimum reaction time for obtaining high conversion and selectivity. Thus, the study showed the time period of 9 h as the optimum reaction time for cinnamaldehyde hydrogenation with respect to the 4-Pd@ZrO₂ catalytic system.

3.3.3. Effects of different solvents on CAL hydrogenation reaction. While studying the effects of different solvents on the catalytic activity towards hydrogenation reactions, few factors need to be taken into consideration such as solvent polarity, easy removal from the reaction system and environmental tolerability.⁷⁴ Water, ethanol, isopropanol, dioxane and toluene were selected for studying their effects on CAL hydrogenation. The reaction process that runs without solvent is always preferred. Hence, initially, the reaction was performed in the absence of a solvent under optimized conditions that resulted in 98% conversion with a moderate yield of HCAL (41%). Furthermore, to enhance the selectivity of the catalyst towards HCAL, the reaction was screened by using different polar and non-polar solvents and the results are displayed in Fig. 12.

To begin with, water, which is considered as a green solvent, was used as a solvent and the reaction was run under similar reaction conditions. The present 4-Pd@ZrO₂ catalytic system in the presence of water yielded 43% HCAL with 100% conversion of CAL. However, HCOL was also obtained with a 35% yield. Instead, the HCAL which is selectively obtained over the 4-Pd@ZrO₂ catalyst undergoes further hydrogenation to form HCOL in the presence of water.⁶⁷ The enhanced adsorption and thus activation of hydrophilic C=O group of HCAL over the catalyst due to the presence of water could possibly be the reason for its further hydrogenation to obtain HCOL. This observation has also been highlighted in the report by Dai *et al.*, wherein the researchers have achieved high selectivity towards COL over PtFe/CNT in the presence of water as a solvent.⁶⁷ This remark suggested that water as a solvent was unable to enhance the catalytic activity of the 4-Pd@ZrO₂ catalyst for the selective

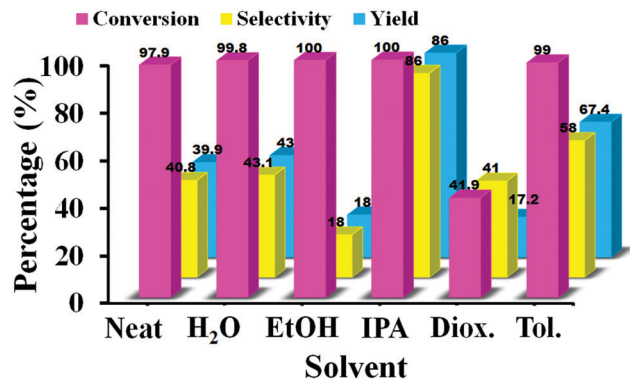


Fig. 12 Catalytic activity study over a Pd@ZrO₂ catalyst with different solvents (reaction conditions: 4-Pd@ZrO₂, 1g CAL, 10 mL solvent, 120 °C temperature, 10 bar H₂, and 9 h).

production of HCAL. Furthermore, ethanol was the choice of solvent as it could easily be separated from the reaction mixture due to its low boiling point. Performing reactions with ethanol did not alter the conversion (100%); however, a drastic drop in the selectivity towards HCAL was observed (18%). The selectivity of HCOL was also not enhanced in the presence of ethanol as a solvent. Hence, the reaction mixture was analyzed for the detection of other side-products which revealed the formation of acetal. It is a known reaction wherein aldehyde and alcohol react to form acetal.⁷⁵ Moreover, acetal forms easily with linear and shorter alcohol such as ethanol as compared to branched alcohol such as isopropanol, due to the steric hindrance effect.⁷⁶ Therefore, the reaction was further tried with IPA as a solvent which interestingly led to 100% conversion with 86% yield towards HCAL. As discussed and proved in the controlled experiments, IPA does not act as a hydrogen donor and the reaction does not follow the transfer hydrogenation pathway.⁶⁷ Most probably, IPA might stabilize the intermediates that lead to the formation of HCAL.

Furthermore, to examine the effects of non-polar solvents on the catalytic activity of the present reaction, the reaction was also performed in the presence of toluene and dioxane as solvents. The conversion in the presence of toluene was 99% and the selectivity towards the desired product was 58%, whereas in the presence of dioxane solvent, both conversion and selectivity decreased to 42% and 41%, respectively. It is reported that non-polar solvents produce saturated aldehydes with high selectivity.⁶⁵ However, moderate selectivity was evidenced in the presence of both the non-polar solvents with the 4-Pd@ZrO₂ catalytic system. Besides, dioxane and toluene solvents are mostly not preferred. The 4Pd@ZrO₂ catalytic system in the presence of IPA as a solvent led to better conversion and selectivity towards HCAL. Moreover, IPA being a volatile solvent can be easily separated and recovered from the reaction mixture which is a crucial factor in terms of academic as well as industrial approach. Therefore, IPA was chosen as a suitable solvent to carry out the reaction in the presence of the 4-Pd@ZrO₂ catalytic system.

3.3.4. Effects of temperature variation on the CAL hydrogenation reaction. It is well known that heat needs to be supplied to most of the catalytic hydrogenation reactions in order to provide enough activation energy so as to drive the reaction in the forward direction.⁶⁵ Hence, the temperature parameter needs to be varied and investigated for its effect on the catalytic hydrogenation of CAL. The temperature was varied between room temperature and 140 °C and the reactions were performed keeping the rest of the parameters constant. The turnover frequency has also been calculated for the 4-Pd@ZrO₂-catalyzed hydrogenation of CAL at different temperatures using the formula [moles of HCAL formed/(no. of active centers × reaction time)] and is displayed in Table 6. On performing the reaction at room temperature, a conversion of 13.1% was obtained with a selectivity of only 8% towards the desired product HCAL (Table 6, entry 1). This result was quite understandable as no external energy in the form of heat was supplied to the system. Hence, a lower TOF of 8.1 h⁻¹ was observed. However, at room temperature, the Pd@ZrO₂ catalyst could produce another product COL with 86% selectivity. When the reaction was performed at 80 °C, not much improvement in conversion (14.3%) and selectivity (14%) was observed. Similarly, a modest TOF was obtained (17.1 h⁻¹) (Table 6, entry 2). Increasing the reaction temperature to 100 °C provided enough energy to activate both the catalyst and the reactant molecule to react which resulted in the conversion of 99.7% with 69.3% selectivity towards HCAL with an increase in TOF (436.5 h⁻¹) (Table 6, entry 3).

Furthermore, by increasing the temperature to 120 °C, 100% conversion was achieved with an 86% yield of HCAL with a higher TOF (710 h⁻¹) (Table 6, entry 4). The effective collisions of the reactant molecules with the active catalyst surface at this temperature could be the reason for the observed conversion and selectivity.⁷⁷ Additionally, the reaction was also performed at 140 °C which showed an increase in the formation of HCOL (19%) and COL (27%) as the by-products, thus decreasing the selectivity towards HCAL (54%) (Table 6, entry 5). There might be a possibility of partial deactivation of the catalyst due to side reactions that usually occur at higher temperatures leading to a decrease in the selectivity of HCAL.⁷⁸ Simultaneously, there was a decrease in the TOF (435.3 h⁻¹). Hence, the temperature study was performed up to 140 °C and the study suggested 120 °C as an optimum temperature for obtaining maximum conversion

Table 6 Catalytic activity study over the 4-Pd@ZrO₂ catalyst at different reaction temperatures^a

Entry	Temperature	Conversion (%)	Selectivity (%)		Yield HCAL ^b (%)	TOF (h ⁻¹)
			HCAL	HCOL		
1	R.T.	13.1	7.8	6.1	1.0	8.1
2	80	14.3	14.1	2.5	2.0	17.1
3	100	99.4	59.6	16	59.2	436.5
4	120	100	86	14	86	710
5	140	100	53.5	18.7	52.8	435.3

^a Reaction conditions: 4-Pd@ZrO₂, 1g CAL, 10 mL IPA, 10 bar H₂, temperature, and 9 h. ^b Calculated by GC.

and selectivity with respect to HCAL. Moreover, the study suggested that the 4-Pd@ZrO₂-catalyzed hydrogenation of cinnamaldehyde followed first-order kinetics with respect to the reaction temperature. This observation with respect to the variation in reaction temperature is also supported by the literature.⁷⁷

3.3.5. Effects of pressure variation on the CAL hydrogenation reaction. Pressure plays a major role in many liquid-phase hydrogenation reactions. It is a known fact that pressure is essentially important in order to enhance the solubility of molecular hydrogen in the reaction system.⁷⁹ Henry's law suggests the linear increase in hydrogen solubility with the increase of pressure.⁷⁹ Thus, the effects of variation in pressure were studied with respect to cinnamaldehyde hydrogenation. The study was performed at different H₂ pressure ranging from 1, 4, 6, 8, 10, 12 and 14 bar in the same high-pressure reactor under similar reaction conditions (1 g CAL and 5 wt% 4-Pd@ZrO₂ catalyst in 10 mL IPA solvent at 120 °C for 9 h) and the obtained results are represented in Table 7. This reaction system under varying pressure was also considered for calculating TOF using the formula [moles of HCAL formed/(no of active centers × reaction time)], which is shown in Table 7.

To begin with, the hydrogenation of cinnamaldehyde was performed under atmospheric pressure in continuous H₂ flow. A good conversion of around 87% was obtained. However, selectivity towards HCAL was negligible (2%) (Table 7, entry 1). A very less TOF (14 h⁻¹) was obtained for this reaction system. The less solubility and hence less availability of hydrogen on the catalyst surface can probably be the reason for this observation.⁷⁹ The H₂ pressure of 4 bar was then applied and maintained for the same reaction which led to the conversion of 95.2% and enhancement in the selectivity towards HCAL (54.3%) with 426.5 h⁻¹ TOF (Table 7, entry 2). An increase in the selectivity, as well as TOF, could clearly be observed as soon as the catalytic system was pressurized with H₂. This emphasizes the importance of pressure on the activity of the catalyst towards the hydrogenation reaction. Furthermore, the reaction was performed at 6 bar and 8 bar H₂ pressure wherein further increase in conversion and selectivity was observed as expected. At 6 bar pressure, 92.5% conversion and 57.2% selectivity were observed with higher TOF (437 h⁻¹) (Table 7, entry 3).

Furthermore, at 8 bar pressure, conversion reached 98% with 62% selectivity (Table 7, entry 4). When the reaction was performed by applying 10 bar pressure, 100% conversion was achieved with 86% HCAL yield (Table 7, entry 5). Furthermore, by increasing the pressure to 12 and 14 bar, a drop in the selectivity towards HCAL was evidenced with a proportional increase in the yield of HCOL (Table 7, entry 6,7). From this study, 10 bar was chosen as an optimized pressure for the reaction under investigation. Furthermore, change in the pressure led to the change in conversion and selectivity which suggested that the system followed first-order kinetics with respect to the change in pressure which can be correlated with the reports in the literature.⁷⁶

3.3.6. Comparative study of 4-Pd@ZrO₂ catalyst with reported catalysts in CAL hydrogenation reaction. The present study not only demonstrates the catalytic performance of 4-Pd@ZrO₂ towards the chemoselective hydrogenation of cinnamaldehyde but also briefly describes its comparative study with the most recent catalytic systems available in the literature for this reaction. The details of the literature studies employed for comparison are mentioned in Table S1 (ESI†). To begin with, the Pd/C catalyst for cinnamaldehyde hydrogenation displayed good conversion and selectivity towards HCAL at lower reaction temperature and pressure (Table S1, ESI,† entry 1).⁸⁰ However, the drawback of this catalyst is that in order to obtain selectivity towards HCAL, it required the presence of additive (potassium acetate) which is not necessary for the present 4-Pd@ZrO₂ catalytic system.⁸⁰ Furthermore, comparing the catalytic performance of 4-Pd@ZrO₂ with 1 wt% Pt/BN inferred an outstanding conversion of about 95% and selectivity of 85% (Table S1, ESI,† entry 2). However, 1 wt.% Pt/BN catalyst was more selective towards COL and not HCAL at high H₂ pressure of 40 bar.⁷⁸ Additionally, to control the hydrogenation capacity of noble-metal-based catalysts, transition metals are known to be used as a poison.¹² Han *et al.* demonstrated controlled selectivity towards HCAL achieved by the addition of Ni to Pd/SBA-15 (Table S1, ESI,† entry 3).¹² It was observed that the Pd/SBA-15 catalyst alone led to around 50% conversion and 50% selectivity.¹² However, the addition of Ni to Pd/SBA-15 enhanced the reactivity and 88% selectivity was achieved towards HCAL.¹² In this work, Ni was used as a poison to achieve admirable activity towards the hydrogenation of cinnamaldehyde and to target hydrocinnamaldehyde as a major product.

In one of the reports on a Pt noble-metal-based catalyst with Sn as a poison, 3 wt% Pt 0.05 wt% Sn/HPZSM-5 showed a good conversion of 100% (Table S1, ESI,† entry 4).⁸¹ However, the authors found that the catalyst was active to produce COL as a major product by applying a high pressure of 20 bar.⁶⁹ Apart from Pd and Pt, Au has also been explored for the selective hydrogenation process of cinnamaldehyde. 1.5 wt% Au/ZnO was employed as a catalyst to achieve a high conversion of 95% and outstanding selectivity of 100% (Table S1, ESI,† entry 5).⁸² However, the product obtained was COL and the catalyst hardly yielded HCAL (5%).⁷⁰ Liao *et al.* reported the synthesis of Au-Cu/CeO₂ by a direct anion exchange method and its

Table 7 Catalytic activity study over the 4-Pd@ZrO₂ catalyst at different H₂ pressures^a

Entry	Pressure (bar)	Conversion (%)	Selectivity (%)		Yield HCAL ^b (%)	TOF (h ⁻¹)
			HCAL	HCOL		
1	1	56.7	2	4.1	2	14
2	4	95.2	54.3	14.0	52	427
3	6	92.5	57.2	9.5	53	437
4	8	97.6	62	12	60	495.0
5	10	100	86	14	86	710
6	12	100	67.0	19.1	67	549.5
7	14	100	44	25	43.1	356.0

^a Reaction conditions: 4-Pd@ZrO₂, 1 g CAL, 10 mL IPA, H₂ pressure, 120 °C temperature, and 9 h. ^b Calculated by GC.

application in cinnamaldehyde hydrogenation resulted in moderate-to-good conversion and selectivity towards hydrocinnamaldehyde (Table S1, ESI,† entry 6).¹¹ It is very well known that gold-catalyzed systems are highly selective towards cinnamyl alcohol and the catalyst properties need to be tuned to switch its selectivity towards HCAL.¹¹ However, high selectivity was obtained over Au-Cu/CeO₂ at the expense of CAL conversion. Another set of a gold-catalyzed system, Au/Mg-Al-CeO₂, was explored for its application in CAL hydrogenation by Tian *et al.* to selectively yield HCAL (Table S1, ESI,† entry 7).¹³ The reaction conditions employed in the reported studies were found to be quite similar to those of the present work. The reason for high activity was attributed to the presence of oxygen vacancies in the catalyst.¹³ However, the cause for the formation of oxygen vacancies was not taken into discussion. Additionally, solely non-noble-metal-based supported catalysts have also been investigated for cinnamaldehyde hydrogenation. In one of the reports, the Ni/TiO₂ catalyst was synthesized by different methods and its activity towards cinnamaldehyde hydrogenation was compared.⁸³ The Ni/TiO₂ catalyst synthesized by chemical reduction was found to display a good conversion of 91%; however, the catalyst was selective towards COL (Table S1, ESI,† entry 8).⁸³

Taking into consideration the recent literature studies for the selective hydrogenation of cinnamaldehyde, it could be inferred that mostly Pd and Au-based catalytic systems have substantiated decent activity to yield HCAL. However, most of the catalytic systems are complex and reactions have been performed under pretty harsh reaction conditions. Furthermore, the detailed information on the mechanistic approach is somewhere lacking. The authors in the present work describe a simple Pd@ZrO₂ catalytic system for the selective CAL hydrogenation with an admirable activity and selectivity demonstrated under moderate reaction conditions which are very well supported by the characterization and experimental evidence.

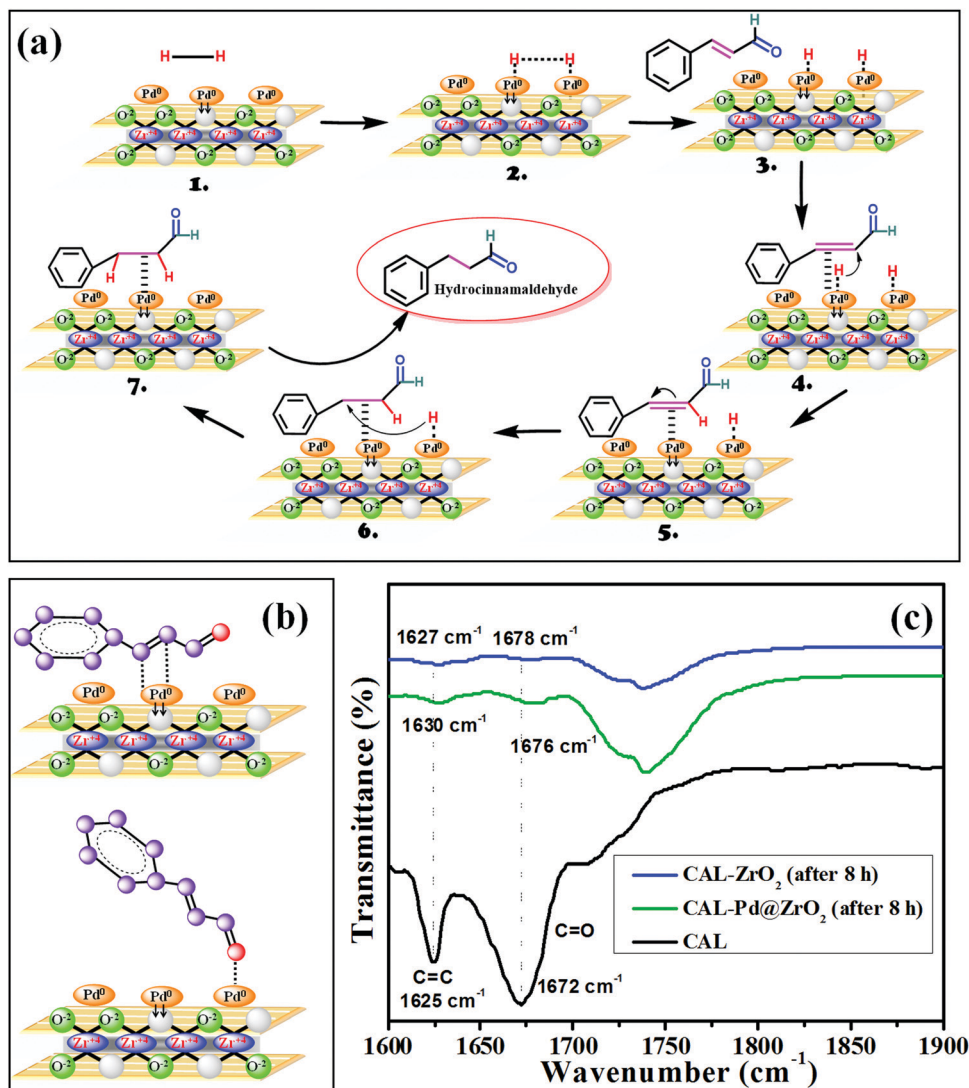
3.3.7. Plausible reaction mechanism for the formation of chemoselective hydrocinnamaldehyde (HCAL) in the presence of an oxygen-vacancy-rich 4-Pd@ZrO₂ catalyst. The present 4-Pd@ZrO₂ catalytic system proved highly efficient in the selective hydrogenation of CAL to HCAL. The activity study revealed that ZrO₂ as a support has a specific role to play in achieving the desired product. Additionally, IPA solvent helps to accelerate the activity and selectivity of the 4-Pd@ZrO₂ catalyst towards CAL hydrogenation. Hence, an effort was made to propose a well-supported and accepted plausible mechanistic pathway for the present reaction occurring in the presence of the 4-Pd@ZrO₂ catalyst represented in Scheme 1(a).

The reduced Pd in the 4-Pd@ZrO₂ catalyst serves as a medium to adsorb molecular hydrogen and desorb it into two hydrogen atoms which remain adsorbed on the catalyst surface (dissociative adsorption) (Steps 1 and 2). The CAL molecule comes in the proximity of the catalyst surface (Step 3). The interaction or the adsorption of the reactant molecule on the catalyst surface will predominantly decide the product to be formed. The adsorption of unsaturated aldehydes on metal surfaces may occur through different adsorption modes as

proposed by Horiuti-Polyani *et al.*⁷⁶ Likewise, as suggested by Huckel calculations, the interaction of the active metal surface with the conjugated C=C bond will be larger as compared to the C=O bond if the d-bandwidth of the metal is narrower.⁷⁶ The metal d-bandwidth of the Pd metal is lower than that of the other noble metals (such as Pt, Ir and Os).⁷⁶ Hence, C=C could favorably be chemisorbed on the 4-Pd@ZrO₂ catalyst surface. Additionally, in the present scenario, the induced oxygen vacancies in the 4-Pd@ZrO₂ catalyst are proficient at decreasing the electron density on the Pd surface by pulling electrons from the Pd metal surface.¹³ The back-bonding interaction of C=C with the Pd surface is thus favored over C=O as this phenomenon may increase the interaction of C=C with respect to the Pd metal surface.¹¹

All these parameters predominantly lead to the adsorption of the olefinic double bond of CAL over the catalyst surface (Step 3).¹³ The different modes of interaction of CAL over the 4-Pd@ZrO₂ catalyst surface are shown in Scheme 1(b). To confirm this adsorption mode of CAL over the present catalytic system, FT-IR studies of CAL-adsorbed catalysts were performed.¹³ The FT-IR spectra of CAL adsorbed Pd@ZrO₂ shown in Scheme 1(c) displayed two peaks, one at 1630 cm⁻¹ ascribed to the conjugated C=C stretching vibration and the other at 1676 cm⁻¹ attributed to the C=O stretching vibration of the CAL molecule. While for CAL, the C=C stretching vibration is centered at 1625 cm⁻¹ and the C=O stretching vibration peak is observed at 1672 cm⁻¹. In general, the literature studies suggest that the shift in the IR vibration of an adsorbed molecule reflects the degree of bond activation and its interaction with the catalytic surface. Additionally, the studies suggest that the change in the bond length may also affect its corresponding vibration frequency.⁸⁴ In the present scenario, there is a possibility of a decrease in the bond length of the C=O and C=C bonds due to their interaction with the catalyst surface, which makes the peak wave number shift to higher values. The shift in the stretching vibration of both C=C and C=O bonds to a higher wavelength in the CAL-adsorbed 4-Pd@ZrO₂ suggests the interaction of the CAL molecule after adsorption by orienting itself in such a way that the C=C bond comes in close proximity of the catalyst surface, as shown in Step 4.¹³ Furthermore, the dissociated hydrogen atom present on the catalyst surface adds to the olefinic double bond (Step 5 and 6). Finally, the selectively hydrogenated product HCAL easily desorbs from the catalyst surface and is replaced by a new CAL reactant molecule (Step 7). This quick release of HCAL from the catalyst surface avoids further hydrogenation to HCOL.

3.3.8. Recyclability studies. Heterogeneous catalysts are recommended due to their efficient recyclability, as this factor is important from an environmental as well as industrial viewpoint.^{17,85-89} The present 4-Pd@ZrO₂ catalytic system was also tested for its efficient recyclability performance in CAL hydrogenation. The first catalytic cycle resulted in 100% conversion with 86% selectivity towards HCAL. The catalyst obtained from the first reaction cycle was recovered by a simple filtration process. The residue was washed three times



Scheme 1 (a) Plausible reaction mechanism for the selective hydrogenation of CAL over the 4-Pd@ZrO₂ catalyst, (b) different modes of interaction of CAL with the 4-Pd@ZrO₂ catalyst and (c) FT-IR of CAL adsorbed on the 4-Pd@ZrO₂ catalyst.

alternatively with ethanol and water. The catalyst was dried at 80 °C for 12 h and prior to its reuse in the reaction, the catalyst was freshly reduced in an H₂ atmosphere at 100 °C for 3 h. The stoichiometric amount of the reactant was taken with respect to the amount of the recycled catalyst for the next reaction cycle. The second catalytic cycle showed consistently 100% conversion with 82% selectivity. Furthermore, after the third cycle, the recycled catalyst was able to achieve 99% conversion with consistency in selectivity (82%). For the fourth catalytic cycle, a conversion of 95% was evidenced with 80% selectivity. Similarly, after the fifth consecutive catalytic cycle, the appreciable activity with 95% conversion and 78% selectivity was demonstrated. The sixth reaction cycle decreased the conversion to 90% and the selectivity dropped to 70%. A drastic drop in the activity of the catalyst was observed after the seventh recycle. Thus, the obtained results displayed that the catalyst could produce consistency in the conversion and selectivity for up to six recycles. The result of recyclability is shown in

Fig. 13(a). Furthermore, the catalyst recovered from the sixth recycle was subjected to various characterization techniques to study the structural and morphological changes taking place in the catalyst.

Initially, XRD analysis was performed for the identification of structural changes in the recycled catalyst and the result is shown in Fig. 13(b). Interestingly, no phase destruction was observed and the XRD patterns were similar to those of the fresh 4-Pd@ZrO₂ catalyst. All the major peaks corresponding to the tetragonal (30.2°, 35.1°, 50.6°, 60.1°, 63.0° and 74.7°) and monoclinic phases (24°, 28.2°, 32.2° and 56°) of ZrO₂ are consistent in the XRD of the recycled catalyst. Additionally, peaks corresponding to PdO were also evidenced in the XRD of the recycled catalyst with a decrease in the intensity of the peaks. The crystallite size calculated for the recycled catalyst was 18.2 nm which suggested the formation of bigger crystallites in the recycled catalyst.^{74,75} Moreover, for investigating any morphological changes in the reused catalyst, FE-SEM analysis

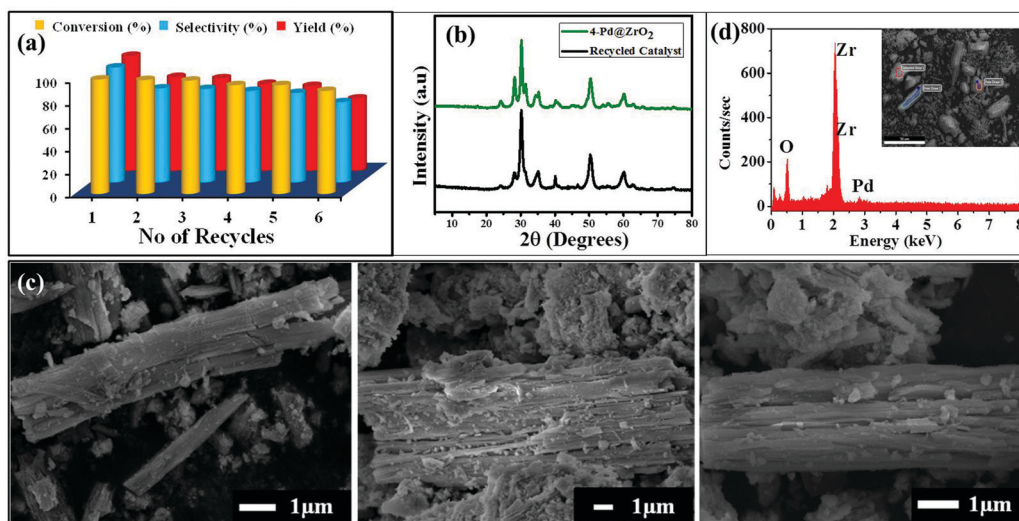


Fig. 13 (a) Recyclability studies over the 4-Pd@ZrO₂ catalyst, (b) XRD of the reused 4-Pd@ZrO₂ catalyst, (c) FE-SEM analysis of the reused 4-Pd@ZrO₂ catalyst and (d) EDX analysis of the reused 4-Pd@ZrO₂ catalyst.

was performed. The rod-like morphology obtained in the fresh 4-Pd@ZrO₂ catalyst was consistent with the morphology of the reused catalyst which is shown in Fig. 13(c). However, the particle size seemed to be slightly increased and was found in the range of 15–20 nm possibly due to the agglomeration of Pd particles to some extent on the surface of the recycled catalyst. This elucidated that the catalyst was structurally very stable even after six recycles. Moreover, the EDX analysis performed for the recycled catalyst is shown in Fig. 13(d). The analysis confirmed the presence of all the elements (Pd, Zr and O) in the required stoichiometry in the recycled catalyst. No other elements were observed which confirmed the purity of the recycled catalyst. Thus, the 4-Pd@ZrO₂ catalyst can be thought of as a highly active, selective and stable catalytic system for the CAL hydrogenation reaction.

4. Conclusion

The present work demonstrated a simple, two-step synthetic protocol to develop oxygen vacancies in various Pd@ZrO₂ catalysts with different Pd loading. We strongly believe that the synthetic approach used in this study to enhance oxygen vacancies in the ZrO₂ support helped to modify the electronic properties of Pd nanoparticles on the 4-Pd@ZrO₂ catalyst, which was confirmed using various characterization techniques. Among the various Pd@ZrO₂ catalysts with different Pd loading tested for the chemoselective hydrogenation of cinnamaldehyde (CAL), the 4-Pd@ZrO₂ catalyst led to the excellent conversion of 100% with 86% selectivity towards hydrocinnamaldehyde (HCAL) under milder reaction conditions. The proposed plausible mechanism revealed that the oxygen-vacancy-rich 4-Pd@ZrO₂ catalyst modified the electronic properties of Pd and influenced the orientation of CAL such that the olefinic bond was selectively hydrogenated to yield hydrocinnamaldehyde. Furthermore, Pd@ZrO₂ catalysts could be recycled up to six cycles

without appreciable loss in their activities and physicochemical properties.

Conflicts of interest

The authors state that there are no conflicts to declare.

Acknowledgements

The authors would like to acknowledge the CNMS, JAIN (Deemed-to-be University) and Nano Mission, DST, Government of India, for their financial support (SR/NM/NS-20/2014). They also gratefully acknowledge the Centre for Nano and Material Sciences (CNMS), JAIN (Deemed-to-be University), Bangalore, for the partial funding support through the basic research grant of JAIN (No. II(39)/17/005/2017SG).

References

- 1 X. Lan and T. Wang, *ACS Catal.*, 2020, **10**, 2764–2790.
- 2 L.-X. Yang, H.-Q. Wu, H.-Y. Gao, J.-Q. Li, Y. Tao, W.-H. Yin and F. Luo, *Inorg. Chem.*, 2018, **57**, 12461–12465.
- 3 X.-M. Liao, V. Pitchon, P.-H. Cuong, W. Chu and V. Caps, *Chin. Chem. Lett.*, 2017, **28**, 293–296.
- 4 S. Han, Y. Liu, J. Li, R. Li, F. Yuan and Y. Zhu, *Catalysts*, 2018, **8**, 200.
- 5 Z. Tian, X. Xiang, L. Xie and F. Li, *Ind. Eng. Chem. Res.*, 2013, **52**, 288–296.
- 6 V. G. Deshmane and Y. G. Adewuyi, *Microporous Mesoporous Mater.*, 2012, **148**, 88–100.
- 7 L. Song, X. Cao and L. Li, *ACS Appl. Mater. Interfaces*, 2018, **10**, 31249–31259.
- 8 W. Xu, J. Wang, L. Wang, G. Sheng, J. Liu, H. Yu and X.-J. Huang, *J. Hazard. Mater.*, 2013, **260**, 498–507.

- 9 J. T. Bhanushali, D. Prasad, K. N. Patil, K. S. Reddy, K. S. R. Rao, A. H. Jadhav and B. M. Nagaraja, *Int. J. Hydrogen Energy*, 2020, **45**, 12874–12888.
- 10 R. L. Austermann, D. R. Denley, D. W. Hart, P. B. Himelfarb, R. M. Irwin, M. Narayana, R. Szentirmay, S. C. Tan and R. C. Yeates, *Anal. Chem.*, 1987, **59**, 68–102.
- 11 J. Chevalier, L. Gremillard, A. V. Virkar and D. R. Clarke, *J. Am. Ceram. Soc.*, 2009, **92**, 1901–1920.
- 12 A. Bumajdad, A. A. Nazeer, F. Al Sagheer, S. Nahar and M. I. Zaki, *Sci. Rep.*, 2018, **8**, 1–9.
- 13 L. J. Durndell, C. M. A. Parlett, N. S. Hondow, M. A. Isaacs, K. Wilson and A. F. Lee, *Sci. Rep.*, 2015, **5**, 9425.
- 14 Z. Yang, Z. Zhu, R. Luo, X. Qiu, J. Liu, J.-K. Yang and W. Tang, *Green Chem.*, 2017, **19**, 3296–3301.
- 15 M.-M. Wang, L. He, Y.-M. Liu, Y. Cao, H.-Y. He and K.-N. Fan, *Green Chem.*, 2011, **13**, 602–607.
- 16 X. Wang, X. Liang, P. Geng and Q. Li, *ACS Catal.*, 2020, **10**, 2395–2412.
- 17 R. Li, H. Chen, Z. Gan, M. Jiang, A. Zhong and H. Bao, *Micro Nano Lett.*, 2018, **13**, 243–247.
- 18 B. Dragoi, I. Mazilu, A. Chiriac, C. Ciotonea, A. Ungureanu, E. Marceau, E. Dumitriu and S. Royer, *Catal. Sci. Technol.*, 2017, **7**, 5376–5385.
- 19 S. Wei, Y. Zhao, G. Fan, L. Yang and F. Li, *Chem. Eng. J.*, 2017, **322**, 234–245.
- 20 Y. Li, P.-F. Zhu and R.-X. Zhou, *Appl. Surf. Sci.*, 2008, **254**, 2609–2614.
- 21 Z. Wang, C. Xu, G. Gao and X. Li, *RSC Adv.*, 2014, **4**, 13644–13651.
- 22 B. Jiang, S. Song, J. Wang, Y. Xie, W. Chu, H. Li, H. Xu, C. Tian and H. Fu, *Nano Res.*, 2014, **7**, 1280–1290.
- 23 E. Hong, C. Kim, D.-H. Lim, H.-J. Cho and C.-H. Shin, *Appl. Catal., B*, 2018, **232**, 544–552.
- 24 X. Guo, *Solid State Ionics*, 1998, **112**, 113–116.
- 25 S. N. Basahel, M. Mokhtar, E. H. Alsharaeh, T. T. Ali, H. A. Mahmoud and K. Narasimharao, *Catalysts*, 2016, **6**, 57.
- 26 O. Akbarzadeh, N. A. Mohd Zabidi, Y. Abdul Wahab, N. A. Hamizi, Z. Z. Chowdhury, Z. M. Aljunid Merican, M. Ab Rahman, S. Akhter, M. Shalauddin and M. R. Johan, *Symmetry*, 2019, **11**, 7.
- 27 S. Zinatloo-Ajabshir and M. Salavati-Niasari, *Int. J. Appl. Ceram. Technol.*, 2016, **13**, 108–115.
- 28 U. Sharma and P. Jeevanandam, *ChemistrySelect*, 2016, **1**, 6382–6395.
- 29 A. Cao, J. Hu and L. Wan, *Sci. China: Chem.*, 2012, **55**, 2249–2256.
- 30 X. Guo, *Chem. Mater.*, 2004, **16**, 3988–3994.
- 31 A. Jalil, S. Triwahyono, N. Sapawe, I. H. Ahmed and M. A. A. Aziz, *Desalin. Water Treat.*, 2015, **56**, 2402–2416.
- 32 L. Kong, I. Karatchevtseva, H. Zhu, M. J. Qin and Z. Aly, *J. Mater. Sci. Technol.*, 2019, **35**, 01966–1976.
- 33 M. S. Santos, J. C. Freitas and C. J. Dalmaschio, *CrystEngComm*, 2020, **22**, 1802–1811.
- 34 C. Colbea, D. Avram, B. Cojocar, R. Negrea, C. Ghica, V. G. Kessler, G. A. Seisenbaeva, V. Parvulescu and C. Tiseanu, *Nanomaterials*, 2018, **8**, 988.
- 35 Y. H. Fang, X. R. Zhao, M. X. Zhang, P. Zhang, L. Zhang, H. Cheng, J. B. Wu and S. S. Feng, *Ceram. Int.*, 2018, **44**, 10094–10098.
- 36 C. Ghosh, D. Ramachandran, G. Balakrishnan, P. Kuppasami and E. Mohandas, *Bull. Mater. Sci.*, 2015, **38**, 401–407.
- 37 L. Li and W. Wang, *Solid State Commun.*, 2003, **127**, 639–643.
- 38 C.-W. Kuo, K.-C. Lee, F.-L. Yen, Y.-H. Shen, H.-E. Lee, S.-B. Wen, M.-C. Wang and M. M. Stack, *J. Alloys Compd.*, 2014, **592**, 288–295.
- 39 J. Zhang, B. Xie, L. Wang, X. Yi, C. Wang, G. Wang, Z. Dai, A. Zheng and F. Xiao, *ChemCatChem*, 2017, **9**, 2661–2667.
- 40 X. Wang, J. Chen, J. Zeng, Q. Wang, Z. Li, R. Qin, C. Wu, Z. Xie and L. Zheng, *Nanoscale*, 2017, **9**, 6643–6648.
- 41 J. Oh, H. B. Bathula, J. H. Park and Y.-W. Suh, *Commun. Chem.*, 2019, **2**, 1–10.
- 42 S. Saleem, R. Ahmad, R. Ayub, U. Ikhlq, W. Jin and P. K. Chu, *Appl. Surf. Sci.*, 2017, **394**, 586–597.
- 43 J. Kim, S. Lee, H. Na, K. Lee and H. Sohn, in *2011 IEEE Int. Interconnect Technol. Conf.*, IEEE, 2011, pp. 1–3.
- 44 M. R. Shaik, M. Alam, S. F. Adil, M. Kuniyil, A. Al-Warthan, M. R. H. Siddiqui, M. N. Tahir, J. P. Labis and M. Khan, *Materials*, 2019, **12**, 711.
- 45 C. V. Reddy, B. Babu, I. N. Reddy and J. Shim, *Ceram. Int.*, 2018, **44**, 6940–6948.
- 46 L. Zhao, J. Zhao, T. Wu, M. Zhao, W. Yan, Y. Zhang, H. Li, Y. Wang, T. Xiao and Y. Zhao, *Nanomaterials*, 2019, **9**, 406.
- 47 S. Jaiswar and K. D. Mandal, *J. Phys. Chem. C*, 2017, **121**, 19586–19601.
- 48 J.-H. Park, J. H. Cho, Y. J. Kim, E. S. Kim, H. S. Han and C.-H. Shin, *Appl. Catal., B*, 2014, **160**, 135–143.
- 49 N. Anbazhagan, G. Imran, A. Qurashi, A. Pandurangan and S. Manimaran, *Microporous Mesoporous Mater.*, 2017, **247**, 190–197.
- 50 W. Q. Zou and R. D. Gonzalez, *J. Catal.*, 1995, **152**, 291–305.
- 51 D. R. Sellick, D. J. Morgan and S. H. Taylor, *Catalysts*, 2015, **5**, 690–702.
- 52 G. Srinivas, V. Krungleviciute, Z.-X. Guo and T. Yildirim, *Energy Environ. Sci.*, 2014, **7**, 335–342.
- 53 K. V. R. Chary, G. V. Sagar, C. S. Srikanth and V. V. Rao, *J. Phys. Chem. B*, 2007, **111**, 543–550.
- 54 A. B. Gaspar, G. R. dos Santos, R. de Souza Costa and M. A. P. da Silva, *Catal. Today*, 2008, **133**, 400–405.
- 55 H. Wang, Y. Chen, Q. Zhang, Q. Zhu, M. Gong and M. Zhao, *J. Nat. Gas Chem.*, 2009, **18**, 211–216.
- 56 J. Jin, C. Li, C.-W. Tsang, B. Xu and C. Liang, *RSC Adv.*, 2015, **5**, 102147–102156.
- 57 J. N. Carstens, S. C. Su and A. T. Bell, *J. Catal.*, 1998, **176**, 136–142.
- 58 Y. Fan, L. Zhang, G. Zhang, H. Xu, Y. Wang and G. Lu, *J. Chin. Chem. Soc.*, 2015, **62**, 117–124.
- 59 X. Cao, A. Mirjalili, J. Wheeler, W. Xie and B. W.-L. Jang, *Front. Chem. Sci. Eng.*, 2015, **9**, 442–449.
- 60 M. Haneda, K. Takamura, Y. Doi, N. Bion and L. Vivier, *J. Mater. Sci.*, 2017, **52**, 5835–5845.

- 61 G. Zafeiropoulos, N. Nikolopoulos, E. Kordouli, L. Sygellou, K. Bourikas, C. Kordulis and A. Lycourghiotis, *Catalysts*, 2019, **9**, 210.
- 62 S. Chen, L. Luo and X. Cheng, 2009, **16**, 272–277.
- 63 F. Drault, C. Comminges, F. Can, L. Pirault-Roy, F. Epron and A. Le Valant, *Materials*, 2018, **11**, 819.
- 64 S. Jayakumar, P. V. Ananthapadmanabhan, K. Perumal, T. K. Thiyagarajan, S. C. Mishra, L. T. Su, A. I. Y. Tok and J. Guo, *Mater. Sci. Eng., B*, 2011, **176**, 894–899.
- 65 L. D'Souza, J. Saleh-Subaie and R. Richards, *J. Colloid Interface Sci.*, 2005, **292**, 476–485.
- 66 M. Lashdaf, M. Tiitta, T. Venäläinen, H. Österholm and A. O. I. Krause, *Catal. Lett.*, 2004, **94**, 7–14.
- 67 M. M. Villaverde, T. F. Garetto and A. J. Marchi, *Catal. Commun.*, 2015, **58**, 6–10.
- 68 J. Zhao, C. Liu, J. Li, R. Wu, J. Wang, H. Qian, H. Guo, J. Li and K. Ibrahim, Oxygen vacancy induced electronic structure variation in the $\text{La}_{0.2}\text{Sr}_{0.8}\text{MnO}_3$ thin film, *AIP Adv.*, 2019, **9**(5), 055208.
- 69 J. M. López, A. L. Gilbank, T. García, B. Solsona, S. Agouram and L. Torrente-Murciano, The prevalence of surface oxygen vacancies over the mobility of bulk oxygen in nanostructured ceria for the total toluene oxidation, *Appl. Catal., B*, 2015, **174**, 403–412.
- 70 L. Zhang, S. Wang and C. Lu, Detection of oxygen vacancies in oxides by defect- dependent cataluminescence, *Anal. Chem.*, 2015, **87**(14), 7313–7320.
- 71 B. M. Reddy, A. Khan, Y. Yamada, T. Kobayashi, S. Loidant and J.-C. Volta, *J. Phys. Chem. B*, 2003, **107**, 11475–11484.
- 72 K. M. Wong, Y. Fang, A. Devaux, L. Wen, J. Huang, L. De Cola and Y. Lei, *Nanoscale*, 2011, **3**, 4830–4839.
- 73 S. Park, H. Kim, C. Jin and C. Lee, *Nanoscale Res. Lett.*, 2011, **6**, 451.
- 74 P. Kluson and L. Cervený, *Appl. Catal., A*, 1995, **128**, 13–31.
- 75 F. Zhao, Y. Ikushima, M. Chatterjee, M. Shirai and M. Arai, *Green Chem.*, 2003, **5**, 76–79.
- 76 R. Basale, *Eindhoven Tech. Univ. Eindhoven*, 2013, 157.
- 77 H. Shi, N. Xu, D. Zhao and B.-Q. Xu, *Catal. Commun.*, 2008, **9**, 1949–1954.
- 78 Z. Cao, J. Bu, Z. Zhong, C. Sun, Q. Zhang, J. Wang, S. Chen and X. Xie, *Appl. Catal., A*, 2019, **578**, 105–115.
- 79 M. Konkol, W. Wróbel, R. Bicki and A. Gołębiowski, *Catalysts*, 2016, **6**, 55.
- 80 Y. Li, H. Cheng, W. Lin, C. Zhang, Q. Wu, F. Zhao and M. Arai, *Catal. Sci. Technol.*, 2018, **8**, 3580–3589.
- 81 Q. Wang, G. Wang, H. Xin, J. Liu, G. Xiong, P. Wu and X. Li, *Catal. Sci. Technol.*, 2019, **9**, 3226–3237.
- 82 H. Chen, D. A. Cullen and J. Z. Larese, *J. Phys. Chem. C*, 2015, **119**, 28885–28894.
- 83 M. G. Prakash, R. Mahalakshmy, K. R. Krishnamurthy and B. Viswanathan, *Catal. Sci. Technol.*, 2015, **5**, 3313–3321.
- 84 J. Ryczkowski, *Catal. Today*, 2001, **68**, 263–381.
- 85 D. Prasad, K. N. Patil, C. R. Chaitra, N. Sandhya, J. T. Bhanushali, S. W. Gosavi, A. H. Jadhav and B. M. Nagaraja, *Appl. Surf. Sci.*, 2019, **488**, 714–727.
- 86 D. Prasad, K. N. Patil, N. Sandhya, C. R. Chaitra, J. T. Bhanushali, A. K. Samal, R. S. Keri, A. H. Jadhav and B. M. Nagaraja, *Appl. Surf. Sci.*, 2019, **489**, 538–551.
- 87 K. N. Patil, D. Prasad, J. T. Bhanushali, H. Kim, A. B. Atar, B. M. Nagaraja and A. H. Jadhav, *Catal. Lett.*, 2020, **150**, 586–604.
- 88 D. Prasad, K. N. Patil, J. T. Bhanushali, B. M. Nagaraja and A. H. Jadhav, *Catal. Sci. Technol.*, 2019, **9**, 4393–4412.
- 89 J. T. Bhanushali, D. Prasad, K. N. Patil, G. V. R. Babu, I. Kainthla, S. R. R. Kamaraju, A. H. Jadhav and B. M. Nagaraja, *New J. Chem.*, 2019, **43**, 11968–11983.